JGP Journal of General Physiology

ARTICLE

Muscle ankyrin repeat protein 1 (MARP1) locks titin to the sarcomeric thin filament and is a passive force regulator

Robbert J. van der Pijl[1,3*], Marloes van den Berg[1,3*], Martijn van de Locht[1], Shengyi Shen[3], Sylvia J.P. Bogaards[1], Stefan Conijn[1], Paul Langlais[4], Pleuni E. Hooijman[1], Siegfried Labeit[5], Leo M.A. Heunks[2], Henk Granzier[3], and Coen A.C. Ottenheijm[1,3]

Muscle ankyrin repeat protein 1 (MARP1) is frequently up-regulated in stressed muscle, but its effect on skeletal muscle function is poorly understood. Here, we focused on its interaction with the titin–N2A element, found in titin's molecular spring region. We show that MARP1 binds to F-actin, and that this interaction is stronger when MARP1 forms a complex with titin–N2A. Mechanics and super-resolution microscopy revealed that MARP1 "locks" titin–N2A to the sarcomeric thin filament, causing increased extension of titin's elastic PEVK element and, importantly, increased passive force. In support of this mechanism, removal of thin filaments abolished the effect of MARP1 on passive force. The clinical relevance of this mechanism was established in diaphragm myofibers of mechanically ventilated rats and of critically ill patients. Thus, MARP1 regulates passive force by locking titin to the thin filament. We propose that in stressed muscle, this mechanism protects the sarcomere from mechanical damage.

Introduction

The smallest contractile unit of striated muscle, the sarcomere, is comprised of three major filaments: the myosin-based thick filaments, the actin-based thin filaments, and the giant filamentous protein titin. Thin and thick filaments interact to produce active force and the titin filaments produces passive force upon sarcomere stretch. This passive force is essential for maintaining the structural integrity of the contracting sarcomere, limiting sarcomere length inhomogeneity along myofibrils, and regulating the level of active force during contraction (Horowits et al., 1986; Fukuda and Granzier, 2005; Fukuda et al., 2005a; Radke et al., 2007; Brynnel et al., 2018; Rivas-Pardo et al., 2020; Swist et al., 2020).

Many proteins are known to interact with the sarcomeric filaments and tune their functional properties (Granzier and Labeit, 2005). Here, we focus on a muscle ankyrin repeat protein 1 (MARP1), also known as Ankrd1/CARP (reviewed in Ling et al., 2017; van der Pijl et al., 2019). MARP1 is of interest as in skeletal muscle it is normally present at very low levels, but its level increases markedly under conditions of mechanical stress (Barash et al., 2004; Witt et al., 2004; Wette et al., 2017; van der Pijl et al., 2018). MARP1 is known to interact with several sarcomere proteins and primarily with the N2A element of titin (Miller et al., 2003; Zhou et al., 2016), found within titin's extensible region that spans from near the sarcomere's Z-disc to near the end of the thick filaments. The N2A element of titin contains four Ig domains and several unique sequences, of which the 104-residue unique sequence (N2A-Us, the sequence to which MARP1 binds) with flanking Ig domains I80 and I81 is a major component (Labeit and Kolmerer, 1995). The importance of the N2A element to muscle health is supported by a mouse model with a spontaneous mutation, resulting in an in-frame deletion of part of I82/I83 in the N2A element (the mdm model) that develops severe myopathy with early death (Garvey et al., 2002; Witt et al., 2004). Additionally, missense mutations in the N2A-Us have been linked to cardiomyopathy (Arimura et al., 2009; Akinrinade et al., 2019), thereby also supporting a critical role of N2A-Us in cardiac health. The N2A element is flanked at its proximal end by a tandem Ig segment (tandemly

[1]Department of Physiology, Amsterdam University Medical Centers, Amsterdam, Netherlands; [2]Intensive Care Medicine, Amsterdam University Medical Centers, Amsterdam, Netherlands; [3]Department of Cellular and Molecular Medicine, University of Arizona, Tuscon, AZ; [4]Division of Endocrinology, University of Arizona, Tucson, AZ; [5]Medical Faculty Mannheim, University of Heidelberg, Mannheim, Germany.

*R.J. van der Pijl and M. van den Berg contributed equally to this paper; Correspondence to Coen A.C. Ottenheijm: coeno@arizona.edu

This work is part of a special collection on myofilament function and disease.

arranged Ig-like domains) that can change length and generate force by unbending of interdomain linker sequences. At the N2A elements distal end is the PEVK segment (proline, glutamate, valine, lysine-rich) that extends greatly and dominates titin's elasticity in intermediate to long sarcomeres (Trombitás et al., 1998a, Trombitás et al., 1998b). These sequences unfold sequentially, starting with the PEVK segment and followed by the tandem Ig repeats at longer sarcomere lengths (reviewed in Granzier and Labeit, 2004). It has been speculated that binding of MARP1 to the N2A element alters titin's stiffness (Miller et al., 2003; Zhou et al., 2016). However, single-molecule studies showed that the direct effect of MARP1 on the elasticity of titin is negligible (Lanzicher et al., 2020).

Here, we study whether MARP1 might indirectly affect passive stiffness by locking titin's N2A element to the thin filament to increase the strain on the remaining free segment of titin and thereby increase force. We perform studies in myofibers of MARP1–3 triple knockout (MKO) mice and diaphragm biopsies of mechanically ventilated humans and rats, and applied various techniques including super-resolution microscopy, myofibril mechanics, and cosedimentation assays with recombinant proteins.

Materials and methods

Mice

Triple knockout mice for Ankrd1, Ankrd2, and Ankrd23, referred to as the MKO, were used (details in Barash et al., 2007). For additional details, see text at the bottom of the PDF.

Patient biopsies

Biopsies from diaphragm muscle were obtained from mechanically ventilated critically ill patients undergoing abdominal or thoracic surgery (critically ill group). The control group consisted of diaphragm biopsies from patients undergoing lung surgery for suspected early-stage lung malignancy. Patients were recruited in the Vrije Universiteit (VU) University Medical Center, Netherlands Cancer Institute–Antoni van Leeuwenhoek Hospital (both in Amsterdam, Netherlands), and Medisch Spectrum Twente (Enschede, Netherlands), and written informed consent was obtained from each patient and/or legal representative (the protocol was approved by the institutional review board at Amsterdam UMC, location VUMC; #2010/69; Hooijman et al., 2014; Hooijman et al., 2015; Lindqvist et al., 2018). For additional information, see text at the bottom of the PDF.

Protein expression and purification

Full-length mouse Ankrd1 (Ensembl accession no. ENSMUST 00000237142.1), human ANKRD1 (Ensembl accession no. ENST 00000371697.4), and titin N2A peptide I80-I81 (Ensembl accession no. ENSMUSG00000051747, exon 101–104) gene sequences were cloned from mouse cDNA or human sequence cloned from a plasmid vector (Lun et al., 2014; for primers, see Table S3). Gene sequences were inserted into pET cloning vectors and inserted into BL21 cells. Details for expression and purification can be found at the bottom of the PDF.

Myofibril mechanics

To study viscoelastic properties, myofibrils isolated from mouse tibialis muscle and diaphragm biopsies were set to an average sarcomere length of 2.2 µm and stretched to 3.0 µm with a speed of 0.5 µm/sarcomere/s. Following baseline passive force measurements, myofibrils were exposed to recombinant GST-mMARP1 and GST-hMARP1, dialyzed into relaxing solution at the following concentrations: 0, 2.5 µg/ml, 25 µg/ml, 54 µg/ml, and 100 µg/ml (0, 38.6, 376.9, 831.0, and 1580 nM, respectively) to determine the dose response curve. Myofibrils were incubated for 3 min with GST-MARP1 before stretching the myofibril to 3 µm. Increase in passive force was determined by subtracting the force determined at baseline (preGST-MARP1). A control experiment was done with GST-only to verify that the effect on passive force was derived from MARP1 and not from protein tags. For additional information and solutions composition, see text at bottom of the PDF.

Fluorescence microscopy

Myofibrils were isolated from m. tibialis cranialis of MKO mice and diaphragm myofibers were isolated from the biopsies. Myofibrils/myofibers were incubated with 0.054 mg/ml MARP1 protein in relaxing solution and stretched to a sarcomere length of 2–3.5 µm in a BSA coated IBIDI µdish with grid. The myofibrils/myofibers were stained with primary antibodies for either N2A (TTN-4 [avian], TTN-PEVK [rabbit]) and MARP1 (ANKRD1-1 [rabbit], Myomedix), and imaged on a Leica TCS SP8 STED 3X (Leica Microsystems). For localization in diaphragm cross sections, 5-µm perpendicular cut diaphragm cryosections were stained with antibodies for MARP1 (goat), MARP1 (rabbit), and MyHC-I (mouse), and covered in vectashield with 6′-diamidino-2-phenylindole (DAPI). Images of the cryosections were obtained with a Zeiss axxiovert inverted digital imaging microscopy workstation (Intelligent Imaging Innovations; 3i). Pictures were analyzed with line scans using ImageJ software (National Institutes of Health). For additional details on staining and antibodies used, see text at bottom of PDF.

Worm-like chain (WLC) modeling

The WLC equation: $FxPL/k_BxT = z/CL + 1/\left[4(1 - z/CL)^2\right] - 1/4$. The WLC model describes the molecule as a deformable continuum of persistence length (PL; a measure of bending rigidity); k_B is Boltzmann's constant, and T is absolute temperature. The PL was taken as 1.4 nm (Labeit et al., 2003). The contour length (CL) of the PEVK segment in mouse tibialis cranialis was assumed at 600 nm (Brynnel et al., 2018) and for human diaphragm fibers 820 nm (Ottenheijm et al., 2006); the relative extension of the PEVK was calculated as z/CL. For fitting, we used Levenberg–Marquardt nonlinear fits of the WLC model (written in IgorPro [Wavemetrics] and KaleidaGraph [Synergy software]). For details, see text at bottom of PDF.

Pull-down assay with GST-mMARP1 and mass spectrometry

To demonstrate that recombinant MARP1 and titin's N2A segment can interact, we performed pulldowns with GST-mMARP1 and N2A [I80-I81]-TST (constructs are shown in Fig. S1).

To determine which proteins interact with MARP1, we performed GST pull-down assays using GST-mMARP1 against mouse muscle lysate derived from C57BL/6J diaphragm muscles. Subsequent SDS-PAGE revealed several MARP1-binding proteins, which were submitted for identification with mass spectrometry (Kruse et al., 2017; Parker et al., 2019). Further details can be found at the bottom of the PDF.

Actin and MARP1–N2A cosedimentation assay

We investigated MARP1 and titin–N2A's ability to bind filamentous skeletal actin using a cosedimentation assay described previously (de Winter et al., 2020). Additional details are in the text at the bottom of the PDF.

SDS gel electrophoresis and Western blotting

SDS-agarose (SDS-AGE) gel electrophoresis and Western blot experiments have been previously described (Greaser and Warren, 2009; van der Pijl et al., 2018). Titin migration distance and bandwidth (full width at half maximum; FWHM) were determined (see Fig. S5 for an illustration of the analysis). Procedures and antibodies used are described in the text at the bottom of the PDF and Table S4.

Diaphragm myofiber passive force measurements

Single diaphragm muscle fibers were isolated from the biopsies, and the cross-sectional area (CSA) and passive force were measured as described previously (Ottenheijm et al., 2008; Ottenheijm et al., 2012). For detailed procedure and solutions used, see text at the bottom of the PDF.

Rat mechanical ventilation

Mechanical ventilation of rats was approved by the Institutional Animal Care and Use Committee of the VU Medical Center (Amsterdam, Netherlands; protocol AVD114002016501) and the University of Arizona (Tucson, AZ). Male rats (mix background of Sprague-Dawley/brown Norway/Fisher 344; n = 8–10) aged 5–6 mo, weighing 400–600 g, were sedated and ventilated as previously described (Lindqvist et al., 2018). See text at the end of the PDF for additional details.

Statistics

Data are presented as mean ± SEM (normally distributed) of the mean or as median with interquartile range (not normally distributed). Unpaired t tests were used to analyze normally distributed continuous measures, and Mann-Whitney tests were used when continuous measures were not normally distributed. A probability value <0.05 was considered statistically significant. *, P < 0.05; **, P < 0.01; ***, P < 0.001; ****, P < 0.0001. Data were analyzed by GraphPad Prism version 7.03 (GraphPad Prism Software).

Online supplemental material

Fig. S1 presents the recombinant constructs and results of F-actin cosedimentation assays with GST-mMARP1 and N2A [I80-I81]-TST. Fig. S2 shows F-actin cosedimentation of the GST-mMARP1 and N2A[I80-I81; Δus]-TST complex. Fig. S3 shows MARP1 levels in supported and controlled mechanically ventilated critically ill patients, and expression of titin-binding proteins in 18 h CMV rats. Fig. S4 displays relative titin protein and phosphorylation levels in critically ill patients compared to controls. Fig. S5 shows titin isoform size and splice variation in human diaphragm biopsies. Fig. S6 displays relative titin protein and phosphorylation levels in 18 h ventilated and control rats. Table S1 contains summarized patient information pertaining to medical history and mechanical ventilation settings. Table S2 contains mass spectrometry data of identified proteins from pull-down assays. Table S3 shows primer data used in this paper. Table S4 lists antibodies used in this paper. Further information on materials and methods can be found at the bottom of the PDF.

Results

MARP1 increases passive force in skeletal muscle of MKO mice

To study whether MARP1 affects passive force of skeletal muscle, we expressed recombinant full-length murine MARP1 (GST-mMARP1; Fig. S1). To rule out that binding of GST-mMARP1 to titin was affected by endogenous MARP1 or its family members MARP2 and MARP3, we performed experiments in myofibrils isolated from m. tibialis cranialis of MKO mice. Myofibrils were used because of their small diameter (~1 µm), which facilitates diffusion of GST-mMARP1 and because in myofibrils the passive force is exclusively generated in the spring elements of titin. Myofibrils were stretched from a sarcomere length of ~2.3 to ~3.0 µm and held at that length for 30 s. In these experiments, we studied the effects at 2.5 µg/ml, 24 µg/ml, 54 µg/ml, and 102 µg/ml (39, 377, 831, and 1,580 nM, respectively) and the passive force was recorded (for a representative recording, see Fig. 1 A). As shown in Fig. 1 B, GST-mMARP1 increased passive force by 50–70%, with a slightly higher effect on the plateau force than on the peak force (n = 12 myofibrils per mMARP1 concentration). The maximal effect on passive force was reached at a [GST-mMARP1] concentration of 831 nM, with no further increase in passive force at 1,580 nM. We propose that at these high concentrations, recombinant MARP1 forms oligomers which might limit the diffusion of MARP1 into the myofibrils. In an independent experiment, we repeated the myofibril-stretch protocol with GST-only protein, which generated curves comparable to those with (–) GST-mMARP1, indicating that the GST-tag alone did not cause the increased passive force with GST-mMARP1. To verify that exposure of the myofibrils to GST-mMARP1 induced binding of MARP1 to N2A, we performed super-resolution optical microscopy with GST-mMARP1 and N2A-epitope antibodies on a subset of myofibrils exposed to GST-mMARP1 (concentration, 831 nM). As shown in Fig. 1 C, MARP1 and N2A colocalized in the myofibrils.

MARP1 reduces extension of titin's proximal tandem Ig segment and increases extension of PEVK

Next, to study whether the increased passive force in myofibrils is due to altered extension of titin's spring elements, we measured the extension of the N2A and PEVK elements in sarcomeres stretched by varying degrees in the presence (831 nM) and absence of GST-mMARP1. For this purpose, stimulated

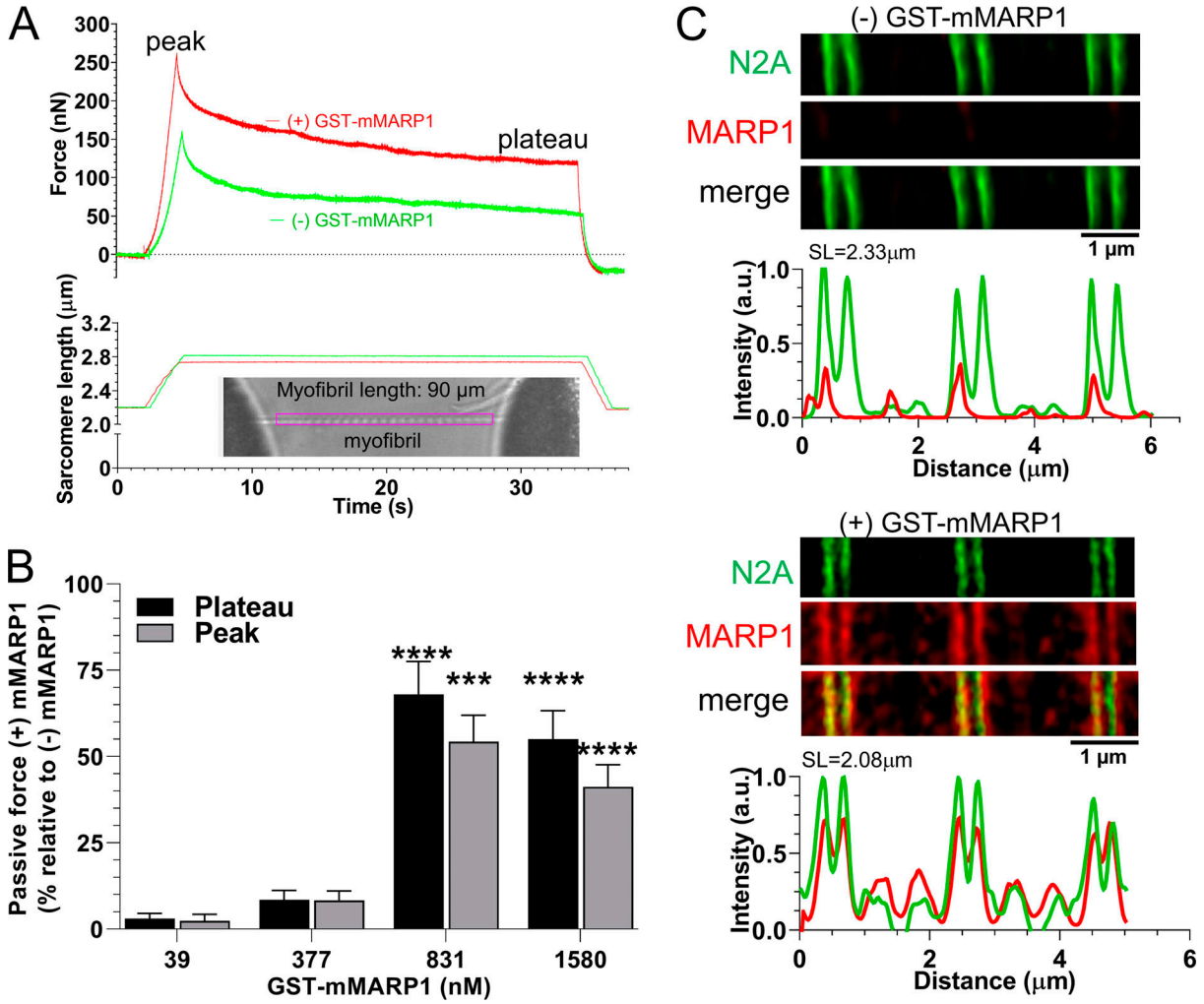

Figure 1. **MARP1 increases passive tension in mouse myofibrils. (A)** Typical force and sarcomere length traces of a stretched myofibril of m. tibialis cranialis of a MKO mouse in the presence and absence of 831 nM GST-mMARP1. Inset shows a typical myofibril mounted in the experimental setup. **(B)** Peak and plateau passive force at various concentrations of GST-mMARP1. Each bar mean ± SEM is the average of 12 myofibrils. **(C)** STED microscopy images of myofibrils exposed to GST-only (top) or GST-mMARP1 (bottom), followed by α-N2A and α-MARP1 antibody staining. Note that N2A and MARP1 colocalize. *T* test relative to (–) GST-mMARP1. ***, P < 0.001; ****, P < 0.0001.

emission depletion (STED) microscopy was used with antibodies that flank the PEVK segment (the N2A [I80-us] antibody and I84-86 antibody, shown in Fig. 2 A). Fig. 2, B and C, show sample images. In myofibrils of the MKO mice, GST-mMARP1 reduced the displacement of the tandem Ig segment element, measured across the Z-disc (Fig. 2 D). Because the total length of the I-band at a given sarcomere length is unchanged, the reduced extension of the tandem Ig segment suggests increased extension of the PEVK segment. Indeed, GST-mMARP1 increased the extension of the PEVK element, as determined by measuring the distance between N2A and I84-86 antibody labeled sites (Fig. 2 E). To estimate the effect of the increased PEVK extension on passive force, we fitted the PEVK data to the WLC model of entropic force generation (see Materials and methods). The CL of the PEVK segment was taken at 600 nm, based on the number of amino acids contained in the PEVK segment of mouse skeletal muscle (Brynnel et al., 2018) and assuming a random coil structure with a maximal residue spacing of 0.38 nm (Watanabe et al., 2002); the fractional extension of the PEVK was calculated as the experimentally determined PEVK extension (Fig. 2 E) divided by the CL. The obtained values were used in the WLC equation, and the force per titin molecule was determined (details in the Materials and methods). The results in Fig. 2 F reveal that MARP1 induces a much steeper force increase with sarcomere extension (P value of slope differences <0.0001).

Thus, MARP1 increases the passive force of sarcomeres by reducing the displacement of N2A from the Z-disc and thereby increasing the fractional extension of the PEVK element. Considering that it requires less time to transcribe/translate the ∼2 kbp ANKRD1 transcript than the ∼109 kbp TTN transcript, this provides a faster mechanism for increasing the passive force of sarcomeres.

MARP1 binds to thin filament proteins, including actin

It was previously found that MARP1 does not alter the extensibility of the titin molecule per se (Lanzicher et al., 2020), and

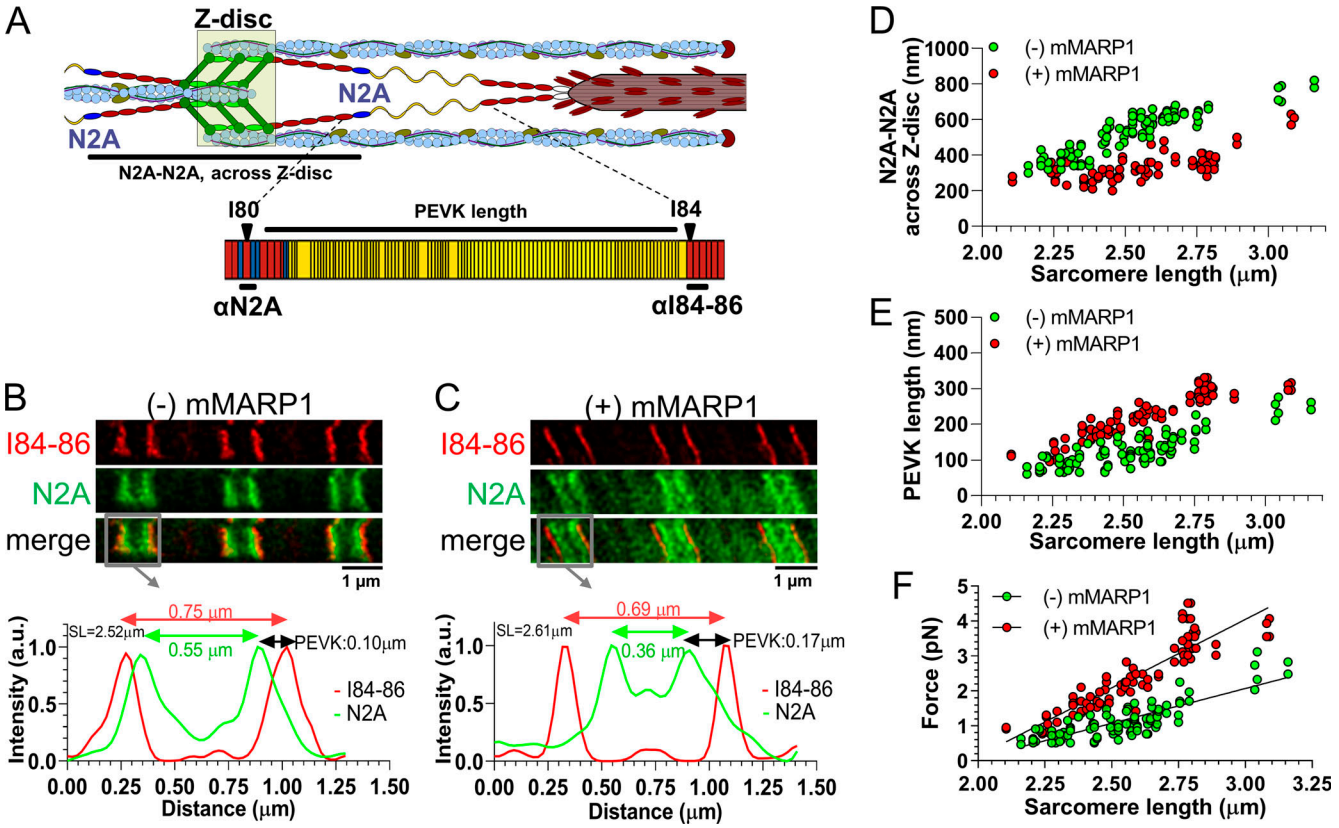

Figure 2. **Epitope distance of titin's N2A and PEVK is shifted in the presence of MARP1. (A)** Schematic of a half sarcomere and titin's N2A and PEVK elements to illustrate the epitopes targeted by the α-N2A and α–I84-86 antibodies. **(B and C)** STED microscopy images of a myofibril not exposed to GST-mMARP1 (B) and a myofibril exposed to GST-mMARP1 (C), followed by α-N2A and α–I84-86 antibody staining. The intensity profiles from the gray boxes highlight the localization of the N2A epitopes (green; arrows peak-peak distance) and the I84-86 epitopes (red; arrows peak-peak distance); the distance between both epitopes reflects the length of the PEVK element. Note that in the intensity profiles, the Z-disc is located in the middle of the intensity peaks. **(D)** The distance between N2A epitopes measured across the Z-disc at various sarcomere lengths. **(E)** PEVK length at various sarcomere lengths. **(F)** Force per titin molecule in the presence and absence of MARP1, as a function of sarcomere length and estimated using a WLC equation. Thus, the increased PEVK extension predicts a large increase in titin-based passive force.

here we discovered that MARP caused a large increase in passive force, accompanied by a reduced tandem Ig segment extension and an increase in PEVK segment extension. This led us to hypothesize that MARP1 locks N2A to the actin filament. To test whether MARP1 binds to thin filament proteins, we performed pull-down assays with GST-mMARP1 and muscle lysates. The pulled-down proteins were separated on an SDS-PAGE gel, and four unique bands were observed (Fig. 3 A). The proteins in these bands were identified by mass spectrometry. All identified proteins are shown in Table S1. Five sarcomeric proteins were identified, including actin, troponin T, and tropomyosin (Fig. 3 B).

Subsequently, to validate that MARP1 binds to actin, we performed cosedimentation assays with MARP1, titin–N2A, and filamentous (F)-actin (recombinant protein constructs are shown in Fig. S1 A). In line with the results of the pull-down assays, the cosedimentation assays showed more GST-mMARP1 pellets in the presence than in the absence of F-actin (Fig. 3 D). GST-only did not sedimentate in the presence or absence of F-actin (Fig. S1 C, top).

To determine whether MARP1 in complex with titin–N2A displays increased affinity for F-actin, compared with MARP1 alone, we expressed two N2A fragments: N2A[I80-I81]-TST, which includes the unique sequence to which MARP1 binds, and a version that lacks the unique sequence between Ig-domain 80-81 (N2A[I80-I81; Δus]-TST; Fig. S1 A). First, we performed GST pull-down experiments with GST-mMARP1 and N2A[I80-I81]-TST and demonstrated that these proteins indeed form a complex in vitro (Fig. 3 C). Cosedimentation of the MARP1–N2A complex showed an increased fraction of GST-mMARP1 in the pellet with F-actin compared with GST-mMARP1 alone (Fig. 3 D), suggesting that the binding of MARP1 to N2A facilitates subsequent binding of complexed MARP1 to F-actin. Interestingly, in the presence of EGTA, the binding of complexed MARP1 to F-actin was even further enhanced, suggesting that Ca^{2+} might reduce binding. The cosedimentation assays with N2A [I80-I81]-TST suggests that N2A also directly binds F-actin in the absence of MARP1 (Fig. S1 C, middle). This interaction is dependent on the unique sequence, as the N2A[I80-I81; Δus]-TST protein did not pellet with F-actin (Fig. S1 C, bottom). Cosedimentation with both GST-mMARP1 and N2A[I80-I81; Δus]-TST also did not enhance GST-mMARP1 sedimentation (Fig. S2), implying that the unique sequence between Ig domain I80-I81 of N2A is indispensable for MARP1–N2A interaction.

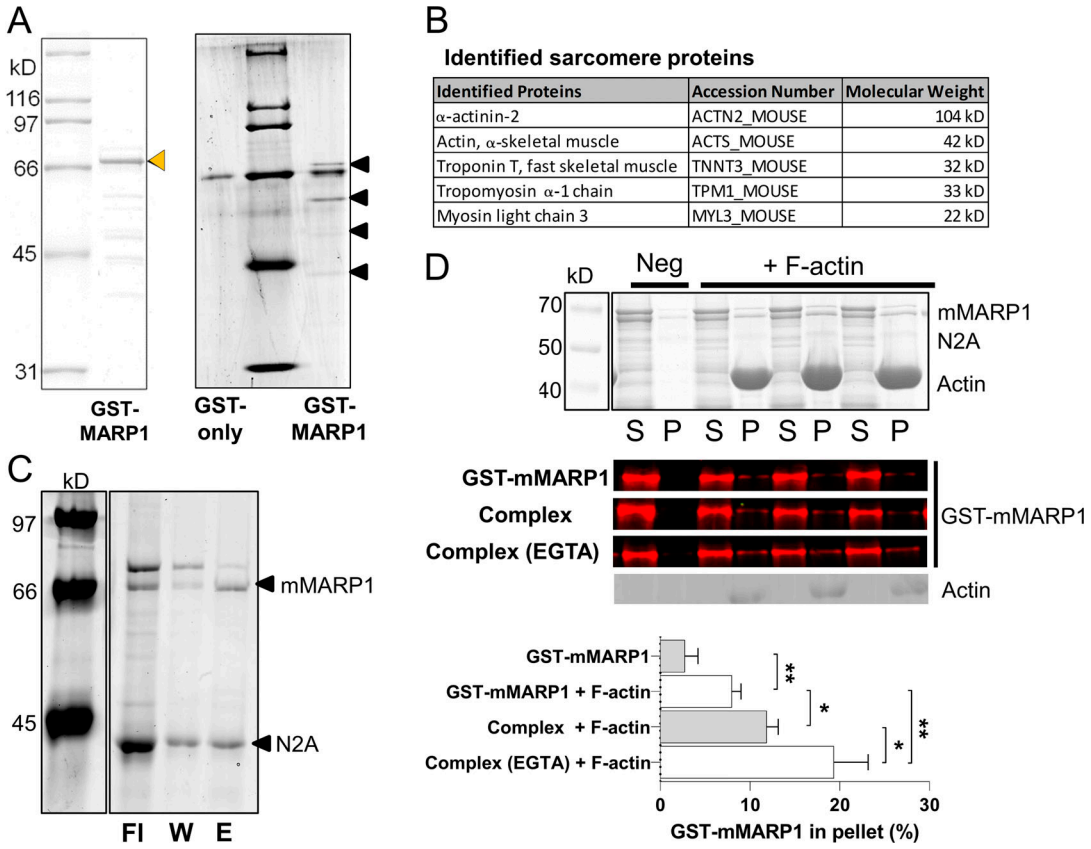

Identified Proteins	Accession Number	Molecular Weight
α-actinin-2	ACTN2_MOUSE	104 kD
Actin, α-skeletal muscle	ACTS_MOUSE	42 kD
Troponin T, fast skeletal muscle	TNNT3_MOUSE	32 kD
Tropomyosin α-1 chain	TPM1_MOUSE	33 kD
Myosin light chain 3	MYL3_MOUSE	22 kD

Figure 3. **GST-pulldown with MARP1 confirms interaction with the actin thin filaments. (A)** Representative gel of GST-mMARP1 (left; orange arrow denotes GST-mMARP1) used for GST pull-down assay. Pull-down in m. tibialis cranialis (A; right) showed four prominent bands (black arrows) of prey pulled by GST-mMARP1. **(B)** The main sarcomeric proteins identified by mass spectrometry in two out of three independent pull-down experiments; for all identified proteins, see Table S1. **(C)** Direct GST-pulldown of the MARP1–N2A complex, GST-mMARP with N2A[I80-I81]-TST (Sumoprotease cleaved). The eluted (E) fraction represents the complex of the two proteins. The noncomplexed fractions are in the flow-through (Fl) and the wash (w). **(D)** Representative gel and Western blots, with GST antibody, of single MARP1 and N2A–MARP1 complex cosedimentation with F-actin, showing increased levels of the complexed MARP1 in the pellet (P) fraction (and corresponding decreased levels in supernatant [S] fraction) with F-actin, compared with the negative control (Neg, no F-actin). Note that in the single GST-mMARP1 lane twice the amount of MARP1 protein (5 μM) was loaded compared with the Complex lane (2.5 μM). The N2A–MARP1 complex showed increased binding to F-actin compared with the individual recombinant proteins (Fig. S1 C) and MARP1 binding while in the complex was further enhanced by the presence of EGTA (20 mM). Bars denote mean ± SEM; three replicates for each cosedimentation assay. *T* test *, P < 0.05; **, P < 0.01.

Thus, binding assays reveal that the MARP1–N2A complex enhances MARP1's affinity for binding to the thin filament.

Removal of the thin filament abolishes the effect of MARP1 on passive force

To test whether the binding of MARP1 to N2A increases passive force by locking titin to the thin filament, we isolated myofibrils from m. tibialis cranialis of MKO mice and exposed the myofibrils for 30 s to a 1.0 M potassium iodide solution. This solution depolymerizes F-actin (Granzier and Irving, 1995; Granzier et al., 1997), and although we cannot rule out that it might affect other sarcomere proteins as well, it leaves titin–N2A in place (Fig. 4 A; n = 5 myofibrils). After removal of the thin filament, the myofibrils were washed, and the myofibril stretch protocol (shown in Fig. 1) was repeated in the absence and presence of 831 nM GST-mMARP1. As shown in Fig. 4, after removal of the thin filament, MARP1 did not increase passive force of sarcomeres. Thus, these findings support that MARP1 locks titin–N2A to the thin filament to increase passive force of sarcomeres.

MARP1 is markedly up-regulated in the diaphragm of critically ill patients

To address the clinical relevance of our findings, we first studied MARP1 levels in diaphragm myofibers of mechanically ventilated critically ill patients (a summary of patients' characteristics, and duration and mode of mechanical ventilation are shown in Table S2). During mechanical ventilation, the diaphragm in these patients undergoes severe reductions in mechanical loading, and we hypothesized MARP1 levels to increase. Control patients were individuals undergoing elective thoracic surgery for removal of a primary lung nodule, during which a diaphragm biopsy was obtained (critically ill patients, n = 28; control patients, n = 22). In line with the hypothesis, we observed an ∼76-fold increase of MARP1 in mechanically ventilated critically ill patients (Fig. 5 A). Other known titin binding proteins showed no difference compared with diaphragm myofibers of control subjects, except for calpain 3, which showed a modest increase in autolytically cleaved fragments (Fig. 5 A). Cross sections showed that the up-regulation of MARP1 occurred

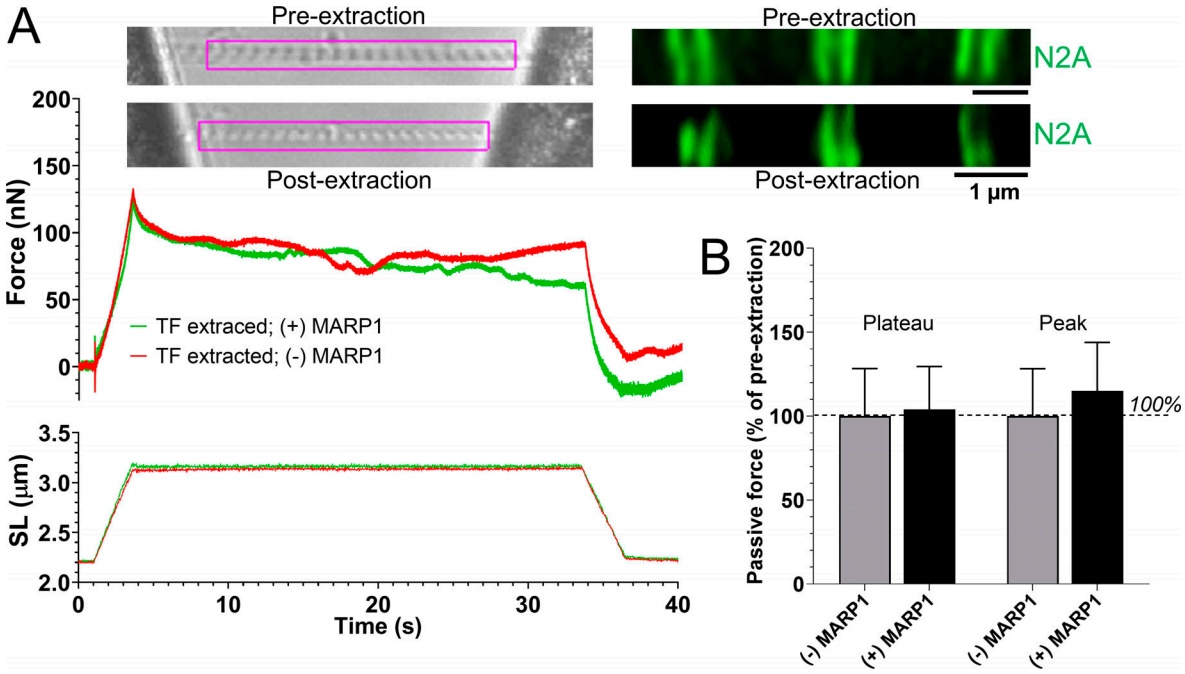

Figure 4. **Thin filament extraction abolishes MARP1-induced passive tension. (A)** Top left: Representative images of an MKO myofibril before and after a 30s exposure to 1.0 M potassium iodide solution to extract the thin filament (TF); note that after extraction, the striation pattern is readily visible. Top right: Confocal imaging shows that after extraction, titin–N2A is still in place. The force and sarcomere length (SL) traces are representative examples of the force and sarcomere length responses to stretch; note that MARP1 does not affect passive force. **(B)** MARP1 does not affect the peak and the plateau force of myofibrils in which the thin filament is extracted (n = 5 myofibrils; mean ± SEM).

equally in slow- and fast-twitch myofibers of critically ill patients, with no nuclear localization (Fig. 5 B). Importantly, super-resolution microscopy studies in longitudinal sections of diaphragm fibers showed that MARP1 and N2A colocalize in critically ill patients (Fig. 5 C).

Critically ill patients on controlled mechanical ventilation (CMV) have a stronger reduction of diaphragm activity than those ventilated with a supportive mode. As a consequence, patients on CMV might have a stronger MARP1 response in the diaphragm. Indeed, we found that MARP1 levels tended to be higher in patients on CMV (P = 0.06; Fig. S3 A), suggesting that diaphragm inactivity may play a role in the up-regulation of MARP1. To assess whether the MARP1 up-regulation in critically ill patients is indeed caused by mechanical ventilation–induced diaphragm unloading, we mechanically ventilated (CMV) healthy rats for 18 h (n = 8–10 per group). In diaphragm tissue of mechanically ventilated rats, MARP1 levels were ∼33-fold higher than in control rats (Fig. S3 B). MARP3 levels were approximately fourfold higher in mechanically ventilated rats. Levels of MARP2, FHL1, MuRF 1, full-length calpain 3, and calpain fragments were not different. Thus, the findings in mechanically ventilated, healthy rats mimic those of mechanically ventilated critically ill patients, suggesting that diaphragm unloading during mechanical ventilation is an important trigger for up-regulation of MARP1.

Note that we found no changes in titin content in the diaphragm of critically ill patients (Fig. S4). Furthermore, titin migration distance and bandwidth (with wider bands reflecting the generation of titin splice variants, resulting in isoforms of variable length) were comparable between control and critically ill patients (Fig. S5), suggesting that in diaphragm myofibers of critically ill patients, no differences occur in titin isoform composition. Finally, total phosphorylation and phosphorylation of PEVK sites S13519 and S13663 were comparable between critically ill and control patients (Figs. S4 and S5). Similar findings were obtained in the mechanically ventilated rats (Fig. S6).

Thus, altogether the analyses of the expression of titin and its binding proteins reveal that MARP1 levels are markedly up-regulated in diaphragm myofibers of critically ill patients.

Reduced extension of the proximal tandem Ig segment and increased PEVK extension in stretched sarcomeres of critically ill patients

We tested whether the high endogenous MARP1 levels in diaphragm myofibers of critically ill patients were associated with reduced extension of the proximal tandem Ig segment and increased extension of the PEVK segment. The extension the proximal tandem Ig segment and PEVK elements was measured in sarcomeres stretched by varying degrees, as described above. Fig. 6 A shows sample images. In myofibrils of critically ill patients, the extension of the tandem Ig segment measured across the Z-disc was reduced (Fig. 6 B) and the extension of the PEVK element was increased (Fig. 6 C). To estimate the effect of the increased PEVK extension on the force generated per titin molecule, we performed similar analyses as described above. We estimated the CL of the PEVK segment in human diaphragm at 820 nm (Ottenheijm et al., 2006). The obtained values were used in the WLC equation, and the force per PEVK segment was

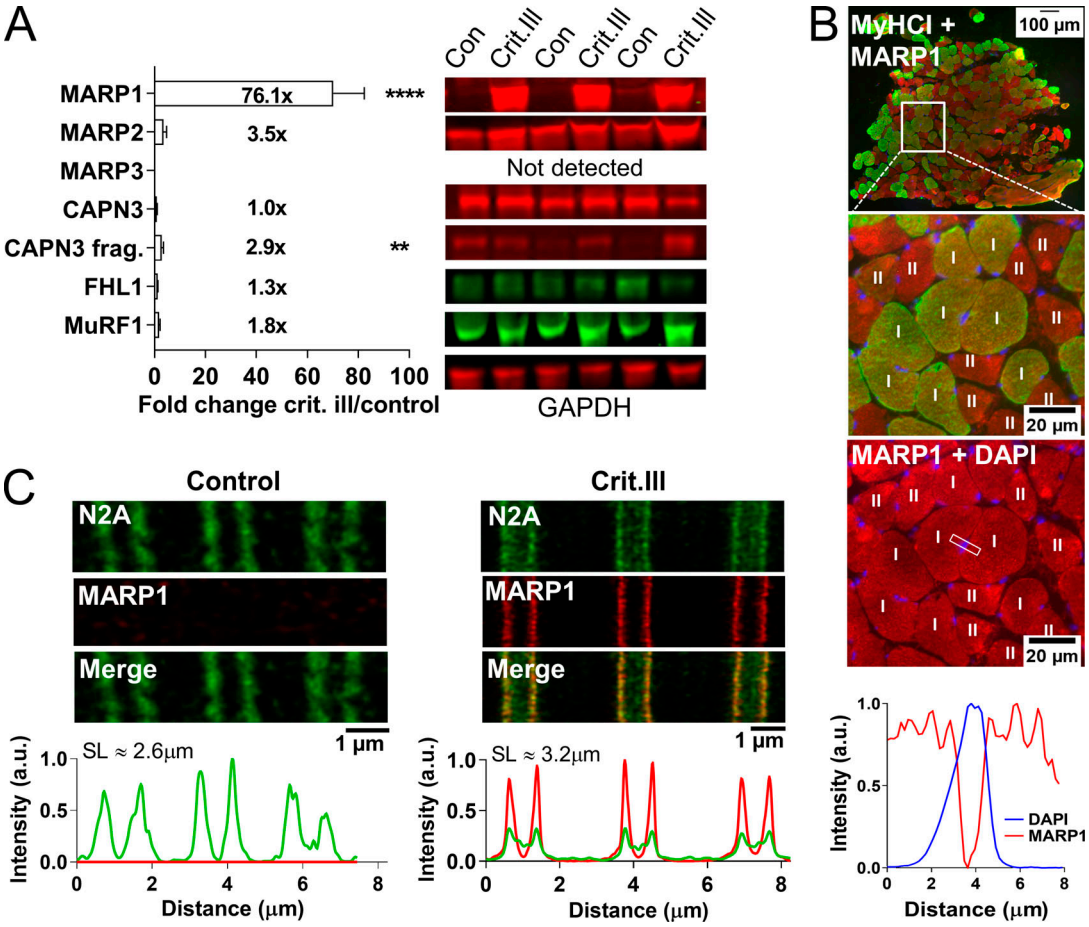

Figure 5. **Expression of titin-binding proteins and localization of MARP1 in diaphragm biopsies of critically ill patients. (A)** Representative examples of diaphragm biopsies of critically ill (n = 21) and control (n = 18) patients analyzed by Western blot and stained with antibodies against MARP1-3, FHL1, CAPN3, MuRF1, and GAPDH. MARP1 was markedly up-regulated in critically ill patients compared with control patients (fold change, 76.1). Full-length calpain 3 was decreased and its autolytic fragments were increased, but no differences in FHL1, MuRF1, and MARP2 were detected. Data are presented as mean ± SEM. FHL, four-and-a-half LIM domains protein 1; MuRF1, muscle ring finger protein 1; CAPN3, calpain 3; P, fragment; Crit.ill, critically ill. **(B)** Cross section of a diaphragm biopsy of a critically ill and control patient stained against MARP1 and MyHC-I. MARP1 was highly present in critically ill patients compared with control patients but was not detectable in the nucleus, and was not fiber-type dependent. MyHC-I, myosin heavy chain I. **(C)** STED microscopy of longitudinal diaphragm myofiber sections of critically ill and control patients stained against MARP1 and titin–N2A. Analysis of the intensity profiles shows colocalization of MARP1 and N2A in myofibers of critically ill patients. SL, sarcomere length. T test relative to control; **, P < 0.01; ****, P < 0.0001.

determined. The results in Fig. 6 D reveal that the PEVK segment in diaphragm myofibers of critically ill patients display a steeper force increase with sarcomere extension. We also experimentally determined the passive force generated by diaphragm myofibers of control and critically ill patients. We analyzed myofibers from 13 control and 20 critically ill patients (8–10 myofibers per patient). Passive force was normalized to the myofiber's CSA (i.e., passive tension) and was higher in myofibers from critically ill compared with control patients (Fig. 6 E).

Thus, our findings suggest that the increased MARP1 levels in diaphragm myofibers of mechanically ventilated critically ill patients increase the extension of the PEVK segment and thereby increase passive force.

Recombinant MARP1 increases passive force in human diaphragm

To verify in an independent study that the increased MARP1 levels in diaphragm myofibers of critically ill patients can mechanistically cause an increased passive force, we isolated single myofibrils from diaphragm muscle of control patients (which have very low, nearly undetectable MARP1 levels; Fig. 5 A) and exposed them to recombinant human MARP1 (GST-hMARP1; concentration, 831 nM, the concentration that yielded a maximal effect in the experiments with mouse myofibrils; Fig. 1 B). Before and after exposure to GST-hMARP1, the myofibrils were stretched from a sarcomere length of ∼2.2 to ∼3.1 µm and held at that length for 60 s. The passive force was recorded (for a representative recording, see Fig. 7 A). As shown in Fig. 7 B, GST-hMARP1 increased the peak and plateau passive force by 40–50%. To verify that exposure of the human myofibrils to GST-hMARP1 induced binding of MARP1 to N2A, we performed super-resolution microscopy with MARP1 and N2A antibodies on a subset of myofibrils exposed to GST-hMARP1 (concentration, 831 nM). As shown in Fig. 6 C, MARP1 and N2A colocalized.

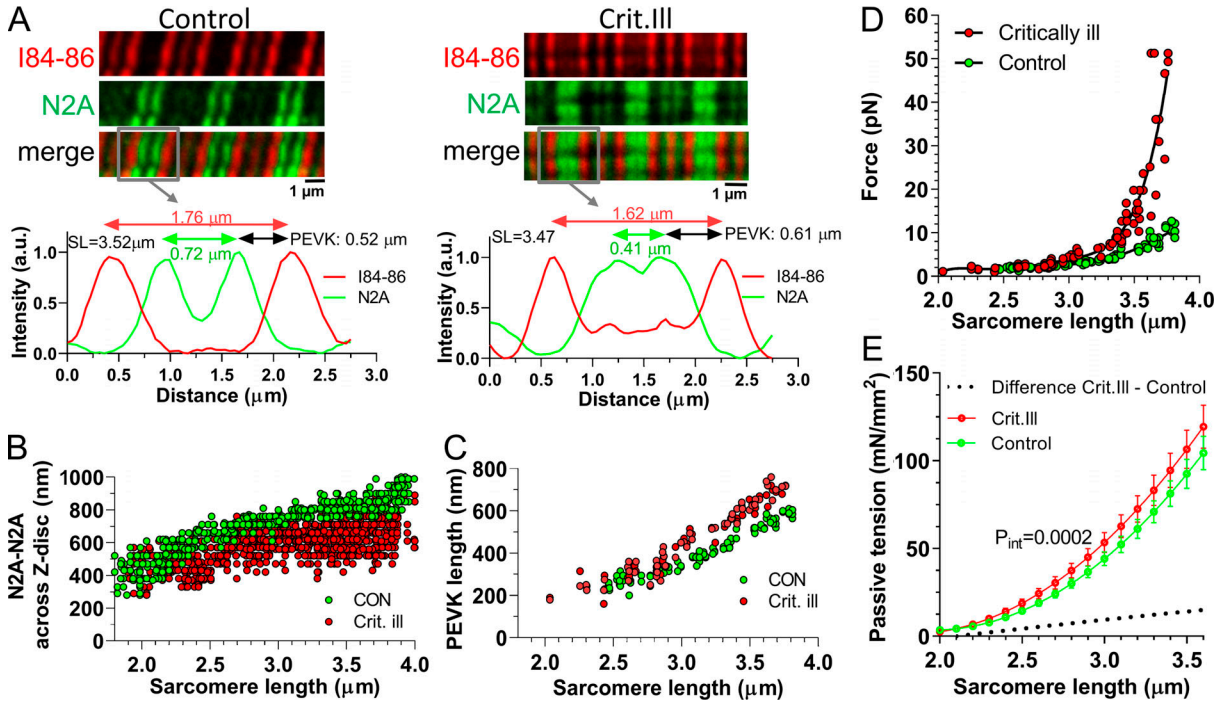

Figure 6. **Epitope distance of titin's N2A and PEVK is shifted in critically ill patients. (A)** Confocal microscopy images of a diaphragm myofibers from a control (left) and a critically ill patient (right) stained with α-N2A and α–I84-86 antibodies. The intensity profiles from the gray boxes highlight the localization of the N2A epitopes (green; arrows peak-peak distance) and the I84-86 epitopes (red; arrows peak-peak distance); the distance between both epitopes reflects the length of the PEVK element. Note that in the intensity profiles the Z-disc is located in the middle of the intensity peaks. **(B)** The distance between N2A epitopes measured across the Z-disc at various sarcomere lengths. **(C)** PEVK length at various sarcomere lengths. **(D)** Force per titin molecule as a function of sarcomere length and estimated using a WLC equation. Thus, the increased PEVK extension predicts an increase in titin-based passive force in critically ill patients. **(E)** Passive tension of single diaphragm myofibers during a stretch from sarcomere 2.0–3.5 µm (mean ± SEM; control n = 13, crit. ill n = 20; 5–10 myofibers per biopsy). Myofibers were stretched with 10% of the fiber length per second and passive force and sarcomere length were measured simultaneously. Passive tension is increased in critically ill patients. Curve comparison, using second order polynomial fit.

Discussion

The data presented in this study provides evidence for a mechanism in which MARP1 locks the N2A element of titin to the thin filament, thereby increasing the fractional extension of the elastic PEVK element during muscle stretch. Consequently, as MARP1 levels increase, the passive force generated by muscle increases as well. This mechanism might provide mechanical stability to sarcomeres during muscle stress.

MARP locks titin–N2A to the thin filament

For optimal structure and function of striated muscle, titin-based elasticity is indispensable (Horowits et al., 1986; Radke et al., 2007; Brynnel et al., 2018; Rivas-Pardo et al., 2020; Swist et al., 2020). During the past two decades, titin's elasticity has been extensively investigated. Titin's elasticity is regulated by posttranscriptional and posttranslational modifications. The posttranscriptional modifications include alternative splicing of titin preMRNA to render molecules with varying lengths of the elastic elements in titin's I-band region (Cazorla et al., 2000; Freiburg et al., 2000; Ottenheijm et al., 2009). Shorter elastic elements will undergo larger fractional extensions during sarcomere stretch and this will increase passive force. Posttranslational modifications include phosphorylation and oxidation of titin's elastic elements (Yamasaki et al., 2002; Fukuda et al., 2005b; Hidalgo et al., 2009; Krüger et al., 2009; Hamdani et al., 2013; Hidalgo and Granzier, 2013; Alegre-Cebollada et al., 2014; Loescher et al., 2020). In addition to posttranscriptional and posttranslational modifications, titin has several binding hotspots for various proteins (reviewed in van der Pijl et al., 2019). A prime example is MARP1. MARP1 binds to titin's N2A element and it has been speculated that its binding affects titin's elasticity (Zhou et al., 2016). However, work in which single-molecule force spectroscopy was applied on the N2A element showed that this element has only a very small effect on the elasticity of titin molecules with no additional effect if MARP1 is bound to N2A (Lanzicher et al., 2020). Here, we show, in agreement with Zhou et al., 2021, that MARP1 decreases titin's elasticity by locking the N2A element to the thin filament (see Fig. 8 for a graphic summary). This locking effect became obvious in experiments in which we stretched sarcomeres in the presence of MARP1 and observed that displacement of the N2A element from the Z-disc was reduced (Fig. 2). Due to this locking, the fractional extension of the PEVK element increases, which increases passive force. Note that at slack sarcomere length (~2.0 µm), the distance between N2A and the Z-disc was ~100 nm (Fig. 2 D), implying that the N2A–MARP1 complex does not directly interact with the Z-disc. Furthermore, myofibrils were incubated while at slack length, and at this short length there was no difference in the N2A–N2A distance between myofibrils incubated with and without MARP1 (Fig. 2 D). During

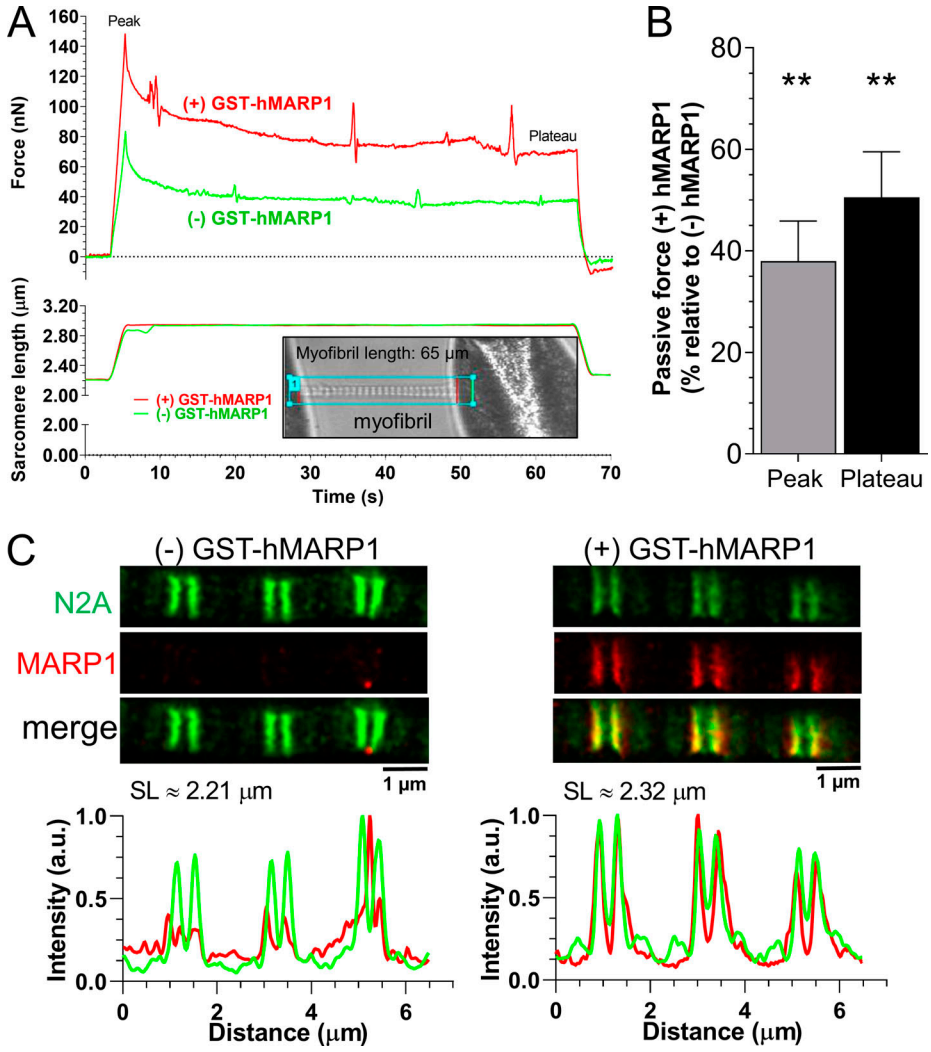

Figure 7. **MARP1 increases passive tension in human diaphragm myofibrils. (A)** Typical force and sarcomere length traces of a stretched myofibril isolated from a diaphragm biopsy of a control patient in the presence and absence of 831 nM GST-hMARP1. Inset shows a typical myofibril mounted in the experimental setup. **(B)** Peak and plateau passive force; bars (mean ± SEM) are the average of 15 myofibrils. **(C)** STED microscopy images of human diaphragm myofibrils exposed to GST-alone (left) or GST-hMARP1 (right), followed by α-N2A and α-MARP1 antibody staining. Note that N2A and MARP1 colocalize. *T* test relative to (–) GST-hMARP1; **, P < 0.01.

stretch to longer lengths, N2A moved relative to the thin filament, but the movement was less than in the absence of MARP1, presumably due to "drag" caused by MARP1. These findings suggest that MARP1 binds titin–N2A to nonspecific locations on the thin filament, and future studies should address this by incubating myofibrils with MARP1 at a range of sarcomere length. The effect of MARP1 on passive force was abolished after removal of the thin filament (Fig. 4), further supporting a concept in which N2A is locked to the thin filament. Pull-down assays and cosedimentation experiments show that MARP1 binds thin filament proteins, including tropomyosin, troponin, and actin, and that the binding affinity for actin is increased when N2A[I80-I81] is present as well (Fig. 3). Thus, we propose that MARP1 acts as "glue" between N2A and the thin filament, as illustrated in Fig. 8. Interestingly, the studies in which myofibrils were stretched after incubation with MARP1 and held at long length for 30 s indicate that the interaction between proteins is remarkably stable. It could be speculated that interactions between MARP1 and troponin and tropomyosin further increase the stability of the binding between titin–N2A and the thin filament.

The cosedimentation assays did not provide evidence for an effect of MARP1 on direct binding of N2A to F-actin. It is known that N2A can bind F-actin (Dutta et al., 2018), which was confirmed in the present study (Fig. S1). However, in complex with MARP1, no increased binding of N2A to F-actin was observed. In contrast to Zhou et al., 2021, we found that more complexed MARP1–N2A bound to F-actin under low-calcium conditions (EGTA; Fig. 3 D). This apparent discrepancy might be due to a difference in the used-peptide fragments. Whereas we used full-length MARP1, Zhou et al. used ANKRD1$^{106–319}$ (encoding the Ank repeats), making their protein more stable in solution, but omitting the PEST region which can also bind titin (Miller et al., 2003) and a coiled-coil domain, which is needed to form MARP

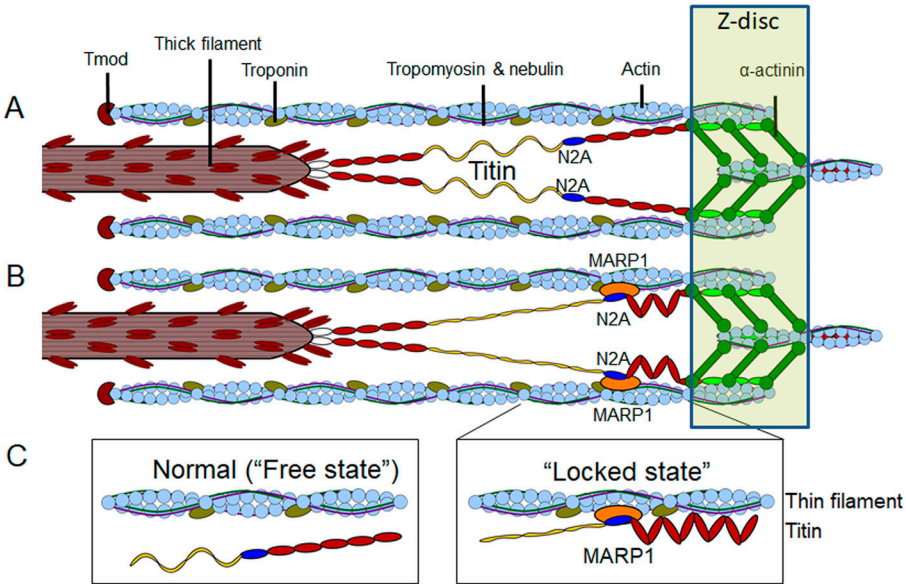

Figure 8. **Graphic summary (not to scale) of the mechanism by which MARP1 locks titin–N2A to the thin filament. (A and B)** The normal or "free state" of the N2A element in healthy unstressed muscle (A) and the "locked state" with MARP1 (orange) gluing titin's N2A element to the thin filament (B). **(C)** Left: Detail of the proposed free and locked states of titin–N2A. Right: immunoglobulin domains in red, N2A-unique sequence in blue, PEVK domains in yellow and fibronectin domains in white.

dimers. Furthermore, our titin fragment consisted of the N2A unique sequence [N2Aus] (flanked by I80 and I81), while Zhou et al. used the N2Aus with or without I81. N2Aus is fairly unstructured (Zhou et al., 2016) and might require its flanking Ig domains for proper folding/function. Although I80 may not be needed for MARP1 binding, its presence might alter the structure of the MARP1–N2A complex, making it more sensitive to calcium.

MARP1 shares ≥50% homology with MARP2 (ankrd2/ARRP) and MARP3 (ankrd23/DARP). Similar to MARP1, MARP2 can bind to titin–N2A, and MARP2 levels are much higher in unstressed skeletal muscle than those of MARP1. Thus, to avoid confounding effects of the presence of endogenous MARP proteins, the studies in which the effect of recombinant mMARP1 was investigated were performed in myofibrils from mice devoid of all MARP proteins (i.e., MKO; Barash et al., 2007). Whether MARP2 is also capable of locking titin–N2A to the thin filament is likely, but has not been tested. Its physiological relevance might be limited, however, as MARP1 has a higher binding affinity for N2A than MARP2 (Miller et al., 2003). MARP2 also does not respond to the same stress cues as MARP1 (Fig. 5 and Fig. S3; van der Pijl et al., 2018; Cenni et al., 2019), suggesting a different function for this protein. MARP3 can also bind to the N2A region but is structurally dissimilar from MARP1 and MARP2. Functionally, it is the least-characterized member of the MARP proteins, and whether it serves a similar function to MARP1 remains to be studied. As we did not detect MARP3 in our human biopsy samples, MARP3 is unlikely to have a cross-linking role like MARP1. MARP3 likely serves metabolic functions (Shimoda et al., 2015) that do not require interactions with titin, and, hypothetically, MARP3 displacement from N2A by MARP1 could facilitate such a function. Competitive binding of the MARPs to N2A have only been tested in vitro (Miller et al., 2003), and it has been shown that N2A can break MARP dimers (Zhou et al., 2016). In vivo, MARP binding to the N2A segment of titin might be regulated by posttranslational modifications. Incidentally, MARP1 can mask a phosphorylation site on N2A (Lanzicher et al., 2020); however, the relevance of this phosphorylation site is currently unknown.

Thus, altogether, the present studies reveal a mechanism for the regulation of passive force, based on MARP1-induced locking of titin–N2A to the thin filament, thereby reducing the extension of the proximal tandem Ig segment and increasing the extension of the elastic PEVK element.

Physiological relevance of the locking mechanism

Under normal conditions, MARP1 is present in skeletal muscle at low concentrations (Wette et al., 2017). Indeed, MARP1 was nearly undetectable with Western blot and immunofluorescence microscopy in diaphragm myofibers of control patients (Fig. 5). Thus, in normal conditions it is unlikely that MARP1-induced locking of titin–N2A to the thin filament is relevant. However, during conditions associated with mechanical stress, such as denervation and myopathies, MARP1 levels in skeletal muscles rise markedly (Tsukamoto et al., 2002; van der Pijl et al., 2018). The locking mechanism will increase passive force, and this will limit overstretch of sarcomeres; it will also increase the slack sarcomere length and increase the restoring force during shortening below the slack length and thereby prevent excessive sarcomere shortening that can be damaging (Helmes et al., 1996). Thus, we propose that in stressed skeletal muscles, the MARP1-induced increase in titin stiffness increases the mechanical integrity of sarcomeres and prevents damage. This new mechanism to regulate passive force is also likely to be relatively fast as it requires less time to transcribe and translate MARP1 than it does to turnover titin and generate stiffer titin isoforms.

To test whether MARP1-induced locking of titin–N2A to the thin filament occurs in stressed human muscles, we turned to a condition associated with extreme diaphragm muscle stress, i.e., mechanical ventilation of critically ill patients. The diaphragm is the most active skeletal muscle in the human body as it contracts during each breath. When critically ill patients are admitted to the intensive care unit, they are mechanically ventilated to support gas exchange in the alveoli. However, the

mechanical ventilation renders the diaphragm inactive, which leads to dramatic structural changes. Degradation pathways are activated, and the diaphragm develops rapid myofiber atrophy and loss of structural integrity (Levine et al., 2008; Hooijman et al., 2015). The resulting diaphragm weakness has a tremendous clinical, economical, and societal impact (Heunks and Ottenheijm, 2018). We found that MARP1 levels were markedly up-regulated in diaphragm myofibers of critically ill patients, an up-regulation caused by diaphragm inactivity as indicated by the studies in ventilated rats (Fig. S3). Importantly, microscopy showed that MARP1 locked N2A to the thin filament in diaphragm sarcomeres of critically ill patients, causing increased PEVK extension and increased passive force. The increase in passive force was modest (Fig. 6 E), which is likely due to the reduced myofibrillar fractional area fraction in diaphragm myofibers of critically ill patients relative to that in control patients (Hooijman et al., 2015). Indeed, consistent with a reduced myofibrillar area, the active tension is also reduced in these myofibers (Hooijman et al., 2014; Hooijman et al., 2015; van den Berg et al., 2017). Nevertheless, caution is warranted as we did not determine endogenous MARP1 concentration in the diaphragm biopsies, relative to that of titin, and therefore we cannot rule out that concentrations were too low to exert an effect on passive force. However, the central role for MARP1 in increasing passive force was supported by extensive studies into titin content and phosphorylation status, which showed no major changes in diaphragm myofibers of critically ill patients (Fig. S4), and by studies in which we showed that recombinant hMARP1 increases passive force in human myofibrils (Fig. 7). We propose that the increased passive force of titin helps maintain the structural integrity of sarcomeres during mechanical stress caused by mechanical ventilation. Furthermore, increased titin-based passive force might improve contractility by reducing myofilament lattice spacing and by structural rearrangements in the thick filament that might promote cross-bridge activation (Fukuda and Granzier, 2005; Ait-Mou et al., 2016).

Whereas the current study indicates a direct role for MARP1 in regulating sarcomere stiffness, previous work suggested a role for MARP1 in muscle trophicity (van der Pijl et al., 2018). Indeed, MARP1 has a nuclear localization signal and interacts with the MLP–PKCα complex and the Erk–GATA4 complex in the heart (Zhong et al., 2015; Lange et al., 2016). Bang et al. (2001a) proposed that the role of MARP1 in trophicity might occur only during muscle development, and that in adult muscle MARP1 is essentially a myofibrillar protein with no nuclear localization. In line with this proposition, in diaphragm myofibers of critically ill patients, while MARP1 levels were high, we did not detect MARP1 in the nuclei (Fig. 5). We cannot rule out that low, undetectable levels of MARP1 do shuttle to the nucleus to affect trophicity pathways in the diaphragm, or that nuclear translocation occurs only during the first hours/days of intensive care unit admission. It is possible that MARP1's function depends on its expression level. High levels of MARP1 (~800 nM; Fig. 1 B) might "activate" its N2A-locking function, whereas low levels (≤400 nM) might predominantly activate MARP1's trophicity-related functions. The pull-down assays with mMARP1 and tissue lysates from healthy mouse muscle suggest minimal interaction with transcription factors, perhaps indicating that in skeletal muscle MARP1 only plays a role in trophicity under very specific conditions or for short periods of time.

Compared with skeletal muscles, in the heart the role of the locking mechanism might be less pronounced but could still be functionally relevant. Although cardiomyopathies are associated with up-regulation of MARP1 (Arber et al., 1997; Aihara et al., 2000; Bang et al., 2014), mutations in MARP1 cause cardiomyopathy (Arimura et al., 2009; Moulik et al., 2009; Crocini et al., 2013), and several mutations in MARP1 alter the binding efficiency to titin's N2A region (Lun et al., 2014), in human left ventricle only 40% of the titin molecules contain the N2A element (Cazorla et al., 2000). This will limit the effect of the mechanism on ventricular structure and function. This effect might be larger in atrial cardiomyocytes as they predominantly express N2A-containing titin isoforms (Cazorla et al., 2000) and increased atrial stretch induces adverse remodeling of atrial myocytes (De Jong et al., 2013). Future studies should address whether in cardiac muscle MARP1 plays a similar role as was discovered in the present study on skeletal muscle.

In summary, the present study provides evidence for a mechanism for tuning the passive force of striated muscle via a MARP1-dependent locking of titin–N2A to the sarcomeric thin filament. This mechanism augments the mechanical integrity of sarcomeres and might help in preserving muscle structure and function during conditions associated with muscle stress.

Acknowledgments

Olaf S. Andersen served as editor.

The authors thank the research nurses, intensivists, and surgeons of the VU Medical Center, Netherlands Cancer Institute–Antoni van Leeuwenhoek, and Medisch Spectrum Twente who were involved with patient inclusion and biopsies. The authors thank Dr. Stephan Lange and Dr. Ju Chen (School of Medicine, University of California, San Diego, San Diego, CA) for providing the MARP1-3 triple KO mice.

Research reported in this work was supported by National Institutes of Health/National Heart, Lung, and Blood Institute grant R01HL121500 (to C.A.C. Ottenheijm), Marie Skłodowska-Curie Research and Innovation Staff Exchange 2014 project 645648 (Muscle Stress Relief; to C.A.C. Ottenheijm and S. Labeit), National Institutes of Health/National Heart, Lung, and Blood Institute grant R35HL144998 (to H. Granzier), and National Institute of Arthritis and Musculoskeletal and Skin Diseases grant R01AR073179 (to H. Granzier).

The authors declare no competing financial interests.

Author contributions: C.A.C. Ottenheijm and H. Granzier designed the research studies. R.J. van der Pijl, M. van den Berg, M. van de Locht, S. Shen, S.J.P. Bogaards, S. Conjin, and P.E. Hooijman conducted the experiments and acquired the data. M. van den Berg, P.E. Hooijman, and L.M.A. Heunks collected human biopsies. R.J. van der Pijl, M. van den Berg, M. van de Locht, S. Shen, S.J.P. Bogaards, S. Conjin, and P.E. Hooijman analyzed the data. Further assistance in experimental work or writing

was provided by S. Labeit and L.M.A. Hooijman. R.J. van der Pijl, M. van den Berg, H. Granzier, and C.A.C. Ottenheijm wrote the manuscript. All authors revised, reviewed, and approved of the final version of the manuscript.

Submitted: 23 March 2021
Accepted: 19 May 2021

References

Aihara, Y., M. Kurabayashi, Y. Saito, Y. Ohyama, T. Tanaka, S. Takeda, K. Tomaru, K. Sekiguchi, M. Arai, T. Nakamura, and R. Nagai. 2000. Cardiac ankyrin repeat protein is a novel marker of cardiac hypertrophy: role of M-CAT element within the promoter. *Hypertension.* 36: 48–53. https://doi.org/10.1161/01.HYP.36.1.48

Ait-Mou, Y., K. Hsu, G.P. Farman, M. Kumar, M.L. Greaser, T.C. Irving, and P.P. de Tombe. 2016. Titin strain contributes to the Frank-Starling law of the heart by structural rearrangements of both thin- and thick-filament proteins. *Proc. Natl. Acad. Sci. USA.* 113:2306–2311. https://doi.org/10.1073/pnas.1516732113

Akinrinade, O., T. Heliö, R.H. Lekanne Deprez, J.D.H. Jongbloed, L.G. Boven, M.P. van den Berg, Y.M. Pinto, T.P. Alastalo, S. Myllykangas, K.V. Spaendonck-Zwarts, et al. 2019. Relevance of titin missense and non-frameshifting insertions/deletions variants in dilated cardiomyopathy. *Sci. Rep.* 9:4093. https://doi.org/10.1038/s41598-019-39911-x

Alegre-Cebollada, J., P. Kosuri, D. Giganti, E. Eckels, J.A. Rivas-Pardo, N. Hamdani, C.M. Warren, R.J. Solaro, W.A. Linke, and J.M. Fernández. 2014. S-glutathionylation of cryptic cysteines enhances titin elasticity by blocking protein folding. *Cell.* 156:1235–1246. https://doi.org/10.1016/j.cell.2014.01.056

Arber, S., J.J. Hunter, J. Ross Jr., M. Hongo, G. Sansig, J. Borg, J.C. Perriard, K.R. Chien, and P. Caroni. 1997. MLP-deficient mice exhibit a disruption of cardiac cytoarchitectural organization, dilated cardiomyopathy, and heart failure. *Cell.* 88:393–403. https://doi.org/10.1016/S0092-8674(00)81878-4

Arimura, T., J.M. Bos, A. Sato, T. Kubo, H. Okamoto, H. Nishi, H. Harada, Y. Koga, M. Moulik, Y.L. Doi, et al. 2009. Cardiac ankyrin repeat protein gene (ANKRD1) mutations in hypertrophic cardiomyopathy. *J. Am. Coll. Cardiol.* 54:334–342. https://doi.org/10.1016/j.jacc.2008.12.082

Bang, M.L., R.E. Mudry, A.S. McElhinny, K. Trombitás, A.J. Geach, R. Yamasaki, H. Sorimachi, H. Granzier, C.C. Gregorio, and S. Labeit. 2001a. Myopalladin, a novel 145-kilodalton sarcomeric protein with multiple roles in Z-disc and I-band protein assemblies. *J. Cell Biol.* 153:413–428. https://doi.org/10.1083/jcb.153.2.413

Bang, M.L., T. Centner, F. Fornoff, A.J. Geach, M. Gotthardt, M. McNabb, C.C. Witt, D. Labeit, C.C. Gregorio, H. Granzier, and S. Labeit. 2001b. The complete gene sequence of titin, expression of an unusual approximately 700-kDa titin isoform, and its interaction with obscurin identify a novel Z-line to I-band linking system. *Circ. Res.* 89:1065–1072. https://doi.org/10.1161/hh2301.100981

Bang, M.L., Y. Gu, N.D. Dalton, K.L. Peterson, K.R. Chien, and J. Chen. 2014. The muscle ankyrin repeat proteins CARP, Ankrd2, and DARP are not essential for normal cardiac development and function at basal conditions and in response to pressure overload. *PLoS One.* 9:e93638. https://doi.org/10.1371/journal.pone.0093638

Barash, I.A., L. Mathew, A.F. Ryan, J. Chen, and R.L. Lieber. 2004. Rapid muscle-specific gene expression changes after a single bout of eccentric contractions in the mouse. *Am. J. Physiol. Cell Physiol.* 286:C355–C364. https://doi.org/10.1152/ajpcell.00211.2003

Barash, I.A., M.L. Bang, L. Mathew, M.L. Greaser, J. Chen, and R.L. Lieber. 2007. Structural and regulatory roles of muscle ankyrin repeat protein family in skeletal muscle. *Am. J. Physiol. Cell Physiol.* 293:C218–C227. https://doi.org/10.1152/ajpcell.00055.2007

Brynnel, A., Y. Hernandez, B. Kiss, J. Lindqvist, M. Adler, J. Kolb, R. van der Pijl, J. Gohlke, J. Strom, J. Smith, et al. 2018. Downsizing the molecular spring of the giant protein titin reveals that skeletal muscle titin determines passive stiffness and drives longitudinal hypertrophy. *eLife.* 7: e40532. https://doi.org/10.7554/eLife.40532

Cazorla, O., A. Freiburg, M. Helmes, T. Centner, M. McNabb, Y. Wu, K. Trombitás, S. Labeit, and H. Granzier. 2000. Differential expression of cardiac titin isoforms and modulation of cellular stiffness. *Circ. Res.* 86: 59–67. https://doi.org/10.1161/01.RES.86.1.59

Cenni, V., S. Kojic, C. Capanni, G. Faulkner, and G. Lattanzi. 2019. Ankrd2 in mechanotransduction and oxidative stress response in skeletal muscle: New cues for the pathogenesis of muscular laminopathies. *Oxid. Med. Cell. Longev.* 2019. 7318796. https://doi.org/10.1155/2019/7318796

Crocini, C., T. Arimura, S. Reischmann, A. Eder, I. Braren, A. Hansen, T. Eschenhagen, A. Kimura, and L. Carrier. 2013. Impact of ANKRD1 mutations associated with hypertrophic cardiomyopathy on contraction parameters of engineered heart tissue. *Basic Res. Cardiol.* 108:349. https://doi.org/10.1007/s00395-013-0349-x

De Jong, A.M., A.H. Maass, S.U. Oberdorf-Maass, R.A. De Boer, W.H. Van Gilst, and I.C. Van Gelder. 2013. Cyclical stretch induces structural changes in atrial myocytes. *J. Cell. Mol. Med.* 17:743–753. https://doi.org/10.1111/jcmm.12064

de Winter, J.M., J.P. Molenaar, M. Yuen, R. van der Pijl, S. Shen, S. Conijn, M. van de Locht, M. Willigenburg, S.J. Bogaards, E.S. van Kleef, et al. 2020. KBTBD13 is an actin-binding protein that modulates muscle kinetics. *J. Clin. Invest.* 130:754–767. https://doi.org/10.1172/JCI124000

Dutta, S., C. Tsiros, S.L. Sundar, H. Athar, J. Moore, B. Nelson, M.J. Gage, and K. Nishikawa. 2018. Calcium increases titin N2A binding to F-actin and regulated thin filaments. *Sci. Rep.* 8:14575. https://doi.org/10.1038/s41598-018-32952-8

Freiburg, A., K. Trombitas, W. Hell, O. Cazorla, F. Fougerousse, T. Centner, B. Kolmerer, C. Witt, J.S. Beckmann, C.C. Gregorio, et al. 2000. Series of exon-skipping events in the elastic spring region of titin as the structural basis for myofibrillar elastic diversity. *Circ. Res.* 86:1114–1121. https://doi.org/10.1161/01.RES.86.11.1114

Fukuda, N., and H.L. Granzier. 2005. Titin/connectin-based modulation of the Frank-Starling mechanism of the heart. *J. Muscle Res. Cell Motil.* 26: 319–323. https://doi.org/10.1007/s10974-005-9038-1

Fukuda, N., Y. Wu, G. Farman, T.C. Irving, and H. Granzier. 2005a. Titin-based modulation of active tension and interfilament lattice spacing in skinned rat cardiac muscle. *Pflugers Arch.* 449:449–457. https://doi.org/10.1007/s00424-004-1354-6

Fukuda, N., Y. Wu, P. Nair, and H.L. Granzier. 2005b. Phosphorylation of titin modulates passive stiffness of cardiac muscle in a titin isoform-dependent manner. *J. Gen. Physiol.* 125:257–271. https://doi.org/10.1085/jgp.200409177

Garvey, S.M., C. Rajan, A.P. Lerner, W.N. Frankel, and G.A. Cox. 2002. The muscular dystrophy with myositis (mdm) mouse mutation disrupts a skeletal muscle-specific domain of titin. *Genomics.* 79:146–149. https://doi.org/10.1006/geno.2002.6685

Granzier, H.L., and T.C. Irving. 1995. Passive tension in cardiac muscle: contribution of collagen, titin, microtubules, and intermediate filaments. *Biophys. J.* 68:1027–1044. https://doi.org/10.1016/S0006-3495(95)80278-X

Granzier, H.L., and S. Labeit. 2004. The giant protein titin: a major player in myocardial mechanics, signaling, and disease. *Circ. Res.* 94:284–295. https://doi.org/10.1161/01.RES.0000117769.88862.F8

Granzier, H.L., and S. Labeit. 2005. Titin and its associated proteins: the third myofilament system of the sarcomere. *Adv. Protein Chem.* 71:89–119. https://doi.org/10.1016/S0065-3233(04)71003-7

Granzier, H., M. Kellermayer, M. Helmes, and K. Trombitás. 1997. Titin elasticity and mechanism of passive force development in rat cardiac myocytes probed by thin-filament extraction. *Biophys. J.* 73:2043–2053. https://doi.org/10.1016/S0006-3495(97)78234-1

Greaser, M.L., and C.M. Warren. 2009. Efficient electroblotting of very large proteins using a vertical agarose electrophoresis system. *Methods Mol. Biol.* 536:221–227. https://doi.org/10.1007/978-1-59745-542-8_24

Hamdani, N., J. Krysiak, M.M. Kreusser, S. Neef, C.G. Dos Remedios, L.S. Maier, M. Krüger, J. Backs, and W.A. Linke. 2013. Crucial role for Ca^{2+}/calmodulin-dependent protein kinase-II in regulating diastolic stress of normal and failing hearts via titin phosphorylation. *Circ. Res.* 112: 664–674. https://doi.org/10.1161/CIRCRESAHA.111.300105

Helmes, M., K. Trombitás, and H. Granzier. 1996. Titin develops restoring force in rat cardiac myocytes. *Circ. Res.* 79:619–626. https://doi.org/10.1161/01.RES.79.3.619

Heunks, L., and C. Ottenheijm. 2018. Diaphragm-protective mechanical ventilation to improve outcomes in ICU patients? *Am. J. Respir. Crit. Care Med.* 197:150–152. https://doi.org/10.1164/rccm.201710-2002ED

Hidalgo, C., and H. Granzier. 2013. Tuning the molecular giant titin through phosphorylation: role in health and disease. *Trends Cardiovasc. Med.* 23: 165–171. https://doi.org/10.1016/j.tcm.2012.10.005

Hidalgo, C., B. Hudson, J. Bogomolovas, Y. Zhu, B. Anderson, M. Greaser, S. Labeit, and H. Granzier. 2009. PKC phosphorylation of titin's PEVK element: a novel and conserved pathway for modulating myocardial

stiffness. *Circ. Res.* 105:631–638: 17: 638. https://doi.org/10.1161/CIRCRESAHA.109.198465

Hidalgo, C., C. Saripalli, and H.L. Granzier. 2014. Effect of exercise training on post-translational and post-transcriptional regulation of titin stiffness in striated muscle of wild type and IG KO mice. *Arch. Biochem. Biophys.* 552-553:100–107. https://doi.org/10.1016/j.abb.2014.02.010

Hooijman, P.E., A. Beishuizen, M.C. de Waard, F.S. de Man, J.W. Vermeijden, P. Steenvoorde, R.A. Bouwman, W. Lommen, H.W. van Hees, L.M. Heunks, et al. 2014. Diaphragm fiber strength is reduced in critically ill patients and restored by a troponin activator. *Am. J. Respir. Crit. Care Med.* 189:863–865. https://doi.org/10.1164/rccm.201312-2260LE

Hooijman, P.E., A. Beishuizen, C.C. Witt, M.C. de Waard, A.R. Girbes, A.M. Spoelstra-de Man, H.W. Niessen, E. Manders, H.W. van Hees, C.E. van den Brom, et al. 2015. Diaphragm muscle fiber weakness and ubiquitin-proteasome activation in critically ill patients. *Am. J. Respir. Crit. Care Med.* 191:1126–1138. https://doi.org/10.1164/rccm.201412-2214OC

Horowits, R., E.S. Kempner, M.E. Bisher, and R.J. Podolsky. 1986. A physiological role for titin and nebulin in skeletal muscle. *Nature.* 323:160–164. https://doi.org/10.1038/323160a0

Krüger, M., S. Kötter, A. Grützner, P. Lang, C. Andresen, M.M. Redfield, E. Butt, C.G. dos Remedios, and W.A. Linke. 2009. Protein kinase G modulates human myocardial passive stiffness by phosphorylation of the titin springs. *Circ. Res.* 104:87–94. https://doi.org/10.1161/CIRCRESAHA.108.184408

Kruse, R., J. Krantz, N. Barker, R.L. Coletta, R. Rafikov, M. Luo, K. Højlund, L.J. Mandarino, and P.R. Langlais. 2017. Characterization of the CLASP2 protein interaction network identifies SOGA1 as a microtubule-associated protein. *Mol. Cell. Proteomics*. 16:1718–1735. https://doi.org/10.1074/mcp.RA117.000011

Labeit, S., and B. Kolmerer. 1995. Titins: giant proteins in charge of muscle ultrastructure and elasticity. *Science.* 270:293–296. https://doi.org/10.1126/science.270.5234.293

Labeit, D., K. Watanabe, C. Witt, H. Fujita, Y. Wu, S. Lahmers, T. Funck, S. Labeit, and H. Granzier. 2003. Calcium-dependent molecular spring elements in the giant protein titin. *Proc. Natl. Acad. Sci. USA.* 100: 13716–13721. https://doi.org/10.1073/pnas.2235652100

Lange, S., K. Gehmlich, A.S. Lun, J. Blondelle, C. Hooper, N.D. Dalton, E.A. Alvarez, X. Zhang, M.L. Bang, Y.A. Abassi, et al. 2016. MLP and CARP are linked to chronic PKCα signalling in dilated cardiomyopathy. *Nat. Commun.* 7:12120. https://doi.org/10.1038/ncomms12120

Lanzicher, T., T. Zhou, C. Saripalli, V. Keschrumrus, J.E. Smith Iii, O. Mayans, O. Sbaizero, and H. Granzier. 2020. Single-molecule force spectroscopy on the N2A element of titin: Effects of phosphorylation and CARP. *Front. Physiol.* 11:173. https://doi.org/10.3389/fphys.2020.00173

Levine, S., T. Nguyen, N. Taylor, M.E. Friscia, M.T. Budak, P. Rothenberg, J. Zhu, R. Sachdeva, S. Sonnad, L.R. Kaiser, et al. 2008. Rapid disuse atrophy of diaphragm fibers in mechanically ventilated humans. *N. Engl. J. Med.* 358:1327–1335. https://doi.org/10.1056/NEJMoa070447

Lindqvist, J., M. van den Berg, R. van der Pijl, P.E. Hooijman, A. Beishuizen, J. Elshof, M. de Waard, A. Girbes, A. Spoelstra-de Man, Z.H. Shi, et al. 2018. Positive end-expiratory pressure ventilation induces longitudinal atrophy in diaphragm fibers. *Am. J. Respir. Crit. Care Med.* 198:472–485. https://doi.org/10.1164/rccm.201709-1917OC

Ling, S.S.M., Y.T. Chen, J. Wang, A.M. Richards, and O.W. Liew. 2017. Ankyrin repeat domain 1 protein: A functionally pleiotropic protein with cardiac biomarker potential. *Int. J. Mol. Sci.* 18:1362. https://doi.org/10.3390/ijms18071362

Loescher, C.M., M. Breitkreuz, Y. Li, A. Nickel, A. Unger, A. Dietl, A. Schmidt, B.A. Mohamed, S. Kötter, J.P. Schmitt, et al. 2020. Regulation of titin-based cardiac stiffness by unfolded domain oxidation (UnDOx). *Proc. Natl. Acad. Sci. USA.* 117:24545–24556. https://doi.org/10.1073/pnas.2004900117

Lun, A.S., J. Chen, and S. Lange. 2014. Probing muscle ankyrin-repeat protein (MARP) structure and function. *Anat. Rec. (Hoboken).* 297:1615–1629. https://doi.org/10.1002/ar.22968

Miller, M.K., M.L. Bang, C.C. Witt, D. Labeit, C. Trombitas, K. Watanabe, H. Granzier, A.S. McElhinny, C.C. Gregorio, and S. Labeit. 2003. The muscle ankyrin repeat proteins: CARP, ankrd2/Arpp and DARP as a family of titin filament-based stress response molecules. *J. Mol. Biol.* 333:951–964. https://doi.org/10.1016/j.jmb.2003.09.012

Moulik, M., M. Vatta, S.H. Witt, A.M. Arola, R.T. Murphy, W.J. McKenna, A.M. Boriek, K. Oka, S. Labeit, N.E. Bowles, et al. 2009. ANKRD1, the gene encoding cardiac ankyrin repeat protein, is a novel dilated cardiomyopathy gene. *J. Am. Coll. Cardiol.* 54:325–333. https://doi.org/10.1016/j.jacc.2009.02.076

Ottenheijm, C.A., L.M. Heunks, T. Hafmans, P.F. van der Ven, C. Benoist, H. Zhou, S. Labeit, H.L. Granzier, and P.N. Dekhuijzen. 2006. Titin and diaphragm dysfunction in chronic obstructive pulmonary disease. *Am. J. Respir. Crit. Care Med.* 173:527–534. https://doi.org/10.1164/rccm.200507-1056OC

Ottenheijm, C.A., L.M. Heunks, and R.P. Dekhuijzen. 2008. Diaphragm adaptations in patients with COPD. *Respir. Res.* 9:12. https://doi.org/10.1186/1465-9921-9-12

Ottenheijm, C.A., A.M. Knottnerus, D. Buck, X. Luo, K. Greer, A. Hoying, S. Labeit, and H. Granzier. 2009. Tuning passive mechanics through differential splicing of titin during skeletal muscle development. *Biophys. J.* 97:2277–2286. https://doi.org/10.1016/j.bpj.2009.07.041

Ottenheijm, C.A., N.C. Voermans, B.D. Hudson, T. Irving, G.J. Stienen, B.G. van Engelen, and H. Granzier. 2012. Titin-based stiffening of muscle fibers in Ehlers-Danlos Syndrome. *J Appl Physiol (1985).* 112:1157–1165. https://doi.org/10.1152/japplphysiol.01166.2011

Parker, S.S., J. Krantz, E.A. Kwak, N.K. Barker, C.G. Deer, N.Y. Lee, G. Mouneimne, and P.R. Langlais. 2019. Insulin induces microtubule stabilization and regulates the microtubule plus-end tracking protein network in adipocytes. *Mol. Cell. Proteomics*. 18:1363–1381. https://doi.org/10.1074/mcp.RA119.001450

Radke, M.H., J. Peng, Y. Wu, M. McNabb, O.L. Nelson, H. Granzier, and M. Gotthardt. 2007. Targeted deletion of titin N2B region leads to diastolic dysfunction and cardiac atrophy. *Proc. Natl. Acad. Sci. USA.* 104: 3444–3449. https://doi.org/10.1073/pnas.0608543104

Rivas-Pardo, J.A., Y. Li, Z. Mártonfalvi, R. Tapia-Rojo, A. Unger, Á. Fernández-Trasancos, E. Herrero-Galán, D. Velázquez-Carreras, J.M. Fernández, W.A. Linke, and J. Alegre-Cebollada. 2020. A HaloTag-TEV genetic cassette for mechanical phenotyping of proteins from tissues. *Nat. Commun.* 11:2060. https://doi.org/10.1038/s41467-020-15465-9

Shimoda, Y., K. Matsuo, Y. Kitamura, K. Ono, T. Ueyama, S. Matoba, H. Yamada, T. Wu, J. Chen, N. Emoto, et al. 2015. Diabetes-related ankyrin repeat protein (DARP/Ankrd23) modifies glucose homeostasis by modulating AMPK activity in skeletal muscle. *PLoS One.* 10. e0138624. https://doi.org/10.1371/journal.pone.0138624

Swist, S., A. Unger, Y. Li, A. Vöge, M. von Frieling-Salewsky, Å. Skärlén, N. Cacciani, T. Braun, L. Larsson, and W.A. Linke. 2020. Maintenance of sarcomeric integrity in adult muscle cells crucially depends on Z-disc anchored titin. *Nat. Commun.* 11:4479. https://doi.org/10.1038/s41467-020-18131-2

Trombitás, K., M. Greaser, G. French, and H. Granzier. 1998a. PEVK extension of human soleus muscle titin revealed by immunolabeling with the anti-titin antibody 9D10. *J. Struct. Biol.* 122:188–196. https://doi.org/10.1006/jsbi.1998.3984

Trombitás, K., M. Greaser, S. Labeit, J.P. Jin, M. Kellermayer, M. Helmes, and H. Granzier. 1998b. Titin extensibility in situ: entropic elasticity of permanently folded and permanently unfolded molecular segments. *J. Cell Biol.* 140:853–859. https://doi.org/10.1083/jcb.140.4.853

Tsukamoto, Y., T. Senda, T. Nakano, C. Nakada, T. Hida, N. Ishiguro, G. Kondo, T. Baba, K. Sato, M. Osaki, et al. 2002. Arpp, a new homolog of carp, is preferentially expressed in type 1 skeletal muscle fibers and is markedly induced by denervation. *Lab. Invest.* 82:645–655. https://doi.org/10.1038/labinvest.3780459

van den Berg, M., P.E. Hooijman, A. Beishuizen, M.C. de Waard, M.A. Paul, K.J. Hartemink, H.W.H. van Hees, M.W. Lawlor, L. Brocca, R. Bottinelli, et al. 2017. Diaphragm atrophy and weakness in the absence of mitochondrial dysfunction in the critically ill. *Am. J. Respir. Crit. Care Med.* 196:1544–1558. https://doi.org/10.1164/rccm.201703-0501OC

van der Pijl, R., J. Strom, S. Conijn, J. Lindqvist, S. Labeit, H. Granzier, and C. Ottenheijm. 2018. Titin-based mechanosensing modulates muscle hypertrophy. *J. Cachexia Sarcopenia Muscle.* 9:947–961. https://doi.org/10.1002/jcsm.12319

van der Pijl, R.J., H.L. Granzier, and C.A.C. Ottenheijm. 2019. Diaphragm contractile weakness due to reduced mechanical loading: role of titin. *Am. J. Physiol. Cell Physiol.* 317:C167–C176. https://doi.org/10.1152/ajpcell.00509.2018

Watanabe, K., P. Nair, D. Labeit, M.S. Kellermayer, M. Greaser, S. Labeit, and H. Granzier. 2002. Molecular mechanics of cardiac titin's PEVK and N2B spring elements. *J. Biol. Chem.* 277:11549–11558. https://doi.org/10.1074/jbc.M200356200

Wette, S.G., H.K. Smith, G.D. Lamb, and R.M. Murphy. 2017. Characterization of muscle ankyrin repeat proteins in human skeletal muscle. *Am. J. Physiol. Cell Physiol.* 313:C327–C339. https://doi.org/10.1152/ajpcell.00077.2017

Witt, C.C., Y. Ono, E. Puschmann, M. McNabb, Y. Wu, M. Gotthardt, S.H. Witt, M. Haak, D. Labeit, C.C. Gregorio, et al. 2004. Induction and

myofibrillar targeting of CARP, and suppression of the Nkx2.5 pathway in the MDM mouse with impaired titin-based signaling. *J. Mol. Biol.* 336: 145–154. https://doi.org/10.1016/j.jmb.2003.12.021

Yamasaki, R., Y. Wu, M. McNabb, M. Greaser, S. Labeit, and H. Granzier. 2002. Protein kinase A phosphorylates titin's cardiac-specific N2B domain and reduces passive tension in rat cardiac myocytes. *Circ. Res.* 90:1181–1188. https://doi.org/10.1161/01.RES.0000021115.24712.99

Zhong, L., M. Chiusa, A.G. Cadar, A. Lin, S. Samaras, J.M. Davidson, and C.C. Lim. 2015. Targeted inhibition of ANKRD1 disrupts sarcomeric ERK-GATA4 signal transduction and abrogates phenylephrine-induced cardiomyocyte hypertrophy. *Cardiovasc. Res.* 106:261–271. https://doi.org/10.1093/cvr/cvv108

Zhou, T., J.R. Fleming, B. Franke, J. Bogomolovas, I. Barsukov, D.J. Rigden, S. Labeit, and O. Mayans. 2016. CARP interacts with titin at a unique helical N2A sequence and at the domain Ig81 to form a structured complex. *FEBS Lett.* 590:3098–3110. https://doi.org/10.1002/1873-3468.12362

Zhou, T., J.R. Fleming, S. Lange, A.L. Hessel, J. Bogomolovas, C. Stronczek, D. Grundei, M. Ghassemian, A. Biju, E. Börgeson, et al. 2021. Molecular characterisation of titin N2A and its binding of CARP reveals a titin/actin cross-linking mechanism. *J. Mol. Biol.* 433. 166901. https://doi.org/10.1016/j.jmb.2021.166901

Supplemental material

Mice

Triple knock-out mice for MARP1 (Ankrd1), MARP2 (Ankrd2) and MARP3 (Ankrd23), referred to as MKO, were used (details in Barash al., 2007). 3-mo-old male mice were sedated with 3% isoflurane. Once fully sedated, as determined by non-response to toe-pinch, they were terminated by cervical dislocation. Diaphragm and tibialis muscles were rapidly dissected and flash frozen for subsequent studies. All experiments were done in accordance with the University of Arizona Institutional Animal Care and Use Committee protocol 13-488 and followed the US National Institutes of Health Using Animals in Intramural Research guidelines for animal use.

Patient biopsies

Diaphragm muscle biopsies were obtained from mechanically ventilated critically ill patients undergoing abdominal or thoracic surgery for clinical reasons (critically ill group). As a control group, diaphragm biopsies were obtained from patients undergoing lung surgery for suspected early-stage lung malignancy. The following exclusion criteria were applied: (1) the presence of COPD GOLD III/IV, chronic heart failure NYHA III/IV, pulmonary hypertension NYHA III/IV, neuromuscular disease, or chronic metabolic disease; (2) the chronic use of corticosteroids (>7.5 mg/d for at least 3 mo); (3) >10% weight loss within 6 mo before surgery for tumor removal or admission to the intensive care unit; (4) current or recent chemotherapy and/or radiotherapy. The Medical Ethics Committee of the VU University Medical Center approved the protocol (#2010/69). Patients were recruited in the VU University Medical Center, Netherlands Cancer Institute–Antoni van Leeuwenhoek Hospital (both in Amsterdam, Netherlands), and Medisch Spectrum Twente (Enschede, Netherlands), and written informed consent was obtained from each patient and/or legal representative (Hooijman et al., 2014; Hooijman et al., 2015; Lindqvist et al., 2018).

Diaphragm muscle biopsies were obtained during surgery and cut into smaller pieces, as described previously (Lindqvist et al., 2018). For all biopsies, one part was directly frozen in liquid nitrogen and stored at −80°C for histology experiments, cryosections, and protein analysis. Another part was stored for myofiber mechanics experiments in relax/glycerol (50/50%; vol/vol) with high concentration protease inhibitors (Rx/Gly_{high}; 1.0 mM dithiothreitol [DTT], 0.24 mM PMSF, 0.4 mM leupeptin, and 0.1 mM E64 [1]) and initially placed on a roller band for 24 h at 4°C. Finally, Rx/Gly_{high} was replaced for Rx/Gly with lower concentrations (Rx/Gly_{low}; 1.0 mM DTT, 0.24 mM PMSF, 0.04 mM leupeptin, and 0.01 mM E64) of protease inhibitors and stored at −20°C until used for passive force experiments.

Protein expression and purification

Full-length mouse Ankrd1 (Ensembl accession no. ENSMUST00000237142.1), human ANKRD1 (Ensembl accession no. ENST00000371697.4) and titin–N2A peptide I80-I81 (Ensembl accession no. ENSMUSG00000051747, exon 101–104) gene sequences were cloned from mouse cDNA or human sequence cloned from a plasmid vector (Lun et al., 2014). Titin domain numbering was based on human sequence (Bang et al., 2001b). The DNA sequence was synthesized and inserted into a pET His6 GST TEV LIC cloning vector (Addgene plasmid #29655) or modified form of pET His6 SUMO TEV LIC cloning vector (Addgene plasmid #29711), adding a TEV restriction site and twin strep-tag (StrepII-tag) at the C-terminal end of the expression construct. A titin–N2A peptide devoid of the unique sequence between I80-I81 (N2A [I80-I81;Δus]) was generated by cloning both I80 and I81 separately and fusing the domains during insertion into a cloning vector (In-fusion cloning kit, Takara). All clones were sequence verified by Eton Bioscience (for primers, see Table S3).

BL21 cells were transformed with either empty pET His6 GST TEV LIC cloning vector (GST-only), mouse Ankrd1 (GST-mMARP1), or human Ankrd1 (GST-hMARP1), respectively. Alternatively, we used a pET His6 SUMO TEV LIC TEV TST cloning vector (SUMO-TST only) to clone titin's N2A segment, consisting of I80-I81 (N2A [I80-I81]-TST or I80-I81 with the unique sequence removed (N2A [I80-I81;Δus]-TST). Cells were grown in 300 ml TB medium supplemented with 0.05 mg/ml kanamycin or 0.1 mg/ml ampicillin at 30°C overnight. To induce expression, medium was changed with 300 ml fresh TB medium supplemented with 0.05 mg/ml kanamycin or 0.1 mg/ml ampicillin and 0.2 mM isopropyl β-D9 thiogalactoside, at 16°C overnight. Cell extracts were prepared using a French Pressure Cell Press (EmulsiFlex-C3, Avestin) and purified with Ni-NTA beads (Qiagen). SUMO-TST only, N2A [I80-I81]-TST and N2A [I80-I81; Δus]-TST were further purified with Strep-Tactin XT Superflow beads (IBA). Protein concentration was determined by comparing optical density of known amounts of BSA on SDS-PAGE gels.

Myofibril mechanics

We adapted previously described methods to investigate the viscoelastic properties of myofibrils isolated from snap frozen mouse tibialis muscle and human diaphragm biopsies (Horowits et al., 1986; Radke et al., 2007; Brynnel et al., 2018; Rivas-Pardo et al., 2020). Small sections (2 × 2 mm) were isolated from the muscle, glycerinated for 24 h at −20°C, and stored at −20°C until day of use. On the day of experiments, a small piece of the glycerinated muscle was cut, and the sample was defrosted in relaxing solution (5.89 mM Na^{2+}–adenosine triphosphate, 6.48 mM $MgCl_2$, 40.76 mM K-propionate, 100.00 mM N,N-Bis-(2-hydroxyethyl)-2-

aminoethanesulfonic acid, 6.97 mM ethyleneglycoltetraacetic acid, and 14.50 mM creatine phosphate sodium salt) containing inhibitors (1 M E64, 1 M DTT, 1 M leupeptin, and 1 M PMSF) at 4°C for ∼1 h. The defrosted muscle sample was kept on ice in relaxing solution containing inhibitors (1 M E64, 1 M DTT, 1 M leupeptin, and 1 M PMSF) and gently dissected and cleaned from debris under microscope before homogenization (15 s at 20,000 rpm; Tissue-Tearor, 985370-XL probe, Bio Spec Products Inc.) in fresh relaxing solution containing inhibitors (1 M E64, 1 M DTT, 1 M leupeptin, and 1 M PMSF). This procedure resulted in a solution containing single myofibrils that were transferred into an experimental bath containing relaxing solution at room temperature. A myofibril was chosen for mechanical measurements based on its striated appearance and attached to a rigid glass fiber attached to a cantilevered force probe (OptiForce, IonOptix LLC.; stiffness = 0.7 N/m) and a rigid glass fiber attached to a piezo motor (Mad City Labs Inc.), which imposed computer-controlled length changes on the myofibrils. Throughout the experimental procedures, the myofibrils were imaged with phase-contrast microscopy and a 40× magnification microscope objective. The myofibril length, average sarcomere length, and cross-sectional area were measured at the beginning and consecutive steps of the experiments with a high-speed camera (Myocam-S, IonOptix LLC.) and IonWizard software (IonOptix LLC.). The myofibrils were set to an average sarcomere length of 2.2 µm and stretched to 3.0 µm, causing deflection of the cantilever on the force probe. The deflection of the cantilever was recorded using an interferometer (OptiForce, IonOptix LLC.) and the force (F) can then be calculated with these values: $F = k \bullet V \bullet S = k \bullet \Delta d$, where k is cantilever stiffness (N/m), V is signal, S is sensitivity m/V, and Δd is cantilever displacement (m). Forces were normalized to the myofibril cross-sectional area. During stretch, myofibrils display both viscous and elastic characteristics. This is evident from the curves shown in Figs. 1 A and 7 A. The sharp peak represents both characteristics, whereas the plateau force is a measure of elasticity. Viscosity resists strain linearly. Thus, the force drops after the strain is removed.

Following baseline passive force measurements, myofibrils were exposed to recombinant GST-mMARP1 and GST-hMARP1, dialyzed into relaxing solution at the following concentrations: 0, 2.5 µg/ml, 25 µg/ml, 54 µg/ml, and 100 µg/ml (0, 38.6, 376.9, 831.0 and 1,580 nM, respectively) to determine the dose response curve. Myofibrils were incubated for 3 min with GST-MARP1 before stretching the myofibril from sarcomere length 2.2 to 3.0 µm. Increase in passive force was determined by subtracting the force determined at baseline (pre-GST-MARP1). A control experiment was done with GST-only to verify that the effect on passive force was derived from MARP1 and not from protein tags.

Fluorescence microscopy

STED microscopy on mouse myofibrils and patients' myofibers

Myofibrils were isolated from m. tibialis cranialis of MKO mice and diaphragm myofibers were isolated from the biopsies. Myofibrils/myofibers were incubated with 0.054 mg/ml MARP1 protein in relaxing solution and stretched to a sarcomere length of 2–3.5 µm in a BSA-coated IBIDI µdish with grid. The myofibrils/myofibers were fixated with 2% formalin in relaxing solution for 5 min. After blocking for 1 h with 2% FBS in PBS, the samples were incubated overnight with a primary antibody mix (TTN-4 [avian] and TTN-PEVK [Myomedix]), followed by a secondary antibody mix (Alexa Fluor 488–labeled goat anti-chicken [Thermofisher] and Abberior star 635p-labeled goat anti-rabbit [Abberior]). After thorough washing, the samples were mounted in mowiol and imaged on a Leica TCS SP8 STED 3X (Leica Microsystems) with an oil immersion objective HCX PL APO STD 100× and gated Hybrid detector. Images were corrected for chromatic aberrations and deconvolved using Huygens Professional software (SVI). Line scans were taken perpendicular to the myofibril orientation and peak to peak distance was measured (ImageJ). For MARP1 staining, the samples were incubated with a different primary antibody mix (TTN-4 [avian] and Ankrd1-1 [Myomedix]).

Microscopy on diaphragm cross-sections of patients

To determine whether MARP1 localization is slow-type of fast-type fiber specific and to investigate whether it is present in the nucleus, we stained cryosections of a biopsy from a critically ill patient with 53-fold MARP1 up-regulation. Serial cryosections from 5 µm were cut from the frozen biopsy perpendicular to the diaphragm fiber direction. Cryosections were skinned for 10 min in 0.2% Triton-X100 in PBS. Subsequently, sections were blocked for 1 h in 2% FBS in PBS. A primary antibody mix of goat anti-MARP1, rabbit anti-MARP1, and mouse anti-MyHC-I in PBS was incubated overnight for 1 h. Next, a secondary antibody mix with Alexa Fluor 488 donkey anti-goat, Alexa Fluor 555 donkey anti-rabbit, and Alexa Fluor 647 donkey anti-mouse in PBS was incubated for 2 h. For all antibodies used and dilutions, see Table S4. After skinning, blocking, and antibody incubation, cryosections were washed four times for 2 min. Finally, cryosections were covered in vectashield with DAPI, and a cover glass was mounted and sealed with nail polish. Control cryosections followed the same protocol but lacked primary antibody incubation. Images of the cryosections were obtained with a Zeiss axxiovert inverted digital imaging microscopy workstation (3i) equipped with a motorized stage and multiple fluorescent channels. A cooled charge-coupled device camera (Cooke Sensicam) was used to record images. Exposures, objective, montage, and pixel binning were automatically recorded and stored in memory. Dedicated imaging and analysis software (SlideBook, version 4.2; 3i) was obtained from Intelligent Imaging Innovations. Pictures were analyzed with line scans using ImageJ software (National Institutes of Health).

WLC modeling

To evaluate the effects of the increased extension of the PEVK segment in the presence of MARP1 on the force per titin molecule, we used the experimentally obtained extension (z) of the PEVK segment (mouse, Fig. 2 E; human, Fig. 6 C). The CL of the PEVK segment in mouse tibialis cranialis was assumed to be the same as determined for mouse extensor digitorum longus, soleus, and diaphragm muscle, i.e., 600 nm (Brynnel et al., 2018) and for human diaphragm fibers 820 nm (Ottenheijm et al., 2006); the relative extension of the PEVK was calculated as z/CL. The obtained values were used in the WLC force equation and the force per titin molecule was determined. The WLC equation: $FxPL/k_BxT = z/CL + 1/\left[4(1 - z/CL)^2\right] - 1/4$. The WLC model describes the molecule as a deformable continuum of persistence length PL (a measure of bending rigidity); k_B is Boltzmann's constant, and T is absolute temperature. The PL was taken as 1.4 nm (Labeit et al., 2003). For fitting, we used Levenberg–Marquardt nonlinear fits of the WLC model (written in IgorPro [Wavemetrics] and KaleidaGraph [Synergy software]).

Pull-down assay with GST-mMARP1 and mass spectrometry

Pull-down of MARP1–N2A complex

To demonstrate that recombinant MARP1 and titin's N2A segment can interact, we performed pull-downs with GST-mMARP1 and N2A [I80-I81]-TST (constructs are shown in Fig. S1). First, N2A [I80-I81]-TST was cleaved with 0.2 U/µl Ulp1 (sumoprotease; pFGET19_Ulp1; Addgene plasmid #64697) for 6 h at 30°C, to remove the His6-SUMO tag, and purified by flowing the mixture through Ni-NTA beads to remove Ulp1 (His6-tagged) and His6-SUMO tag. 1 µM GST mMARP1 and N2A [I80-I81]-TST (without His6-SUMO tag) were co-incubated at 4°C for 1 h with mild rotation. 140 µl of the mixture was added to 20 µl of glutathione beads and incubated for 12 h at 4°C with gentle rotation. The flow through and wash solutions were collected to determine the bound and unbound fraction of N2A [I80-I81]-TST. The complex was eluted from the glutathione beads with 8 M urea buffer (50 mM Tris-HCl, 150 mM NaCl, and 8 M urea, pH 8.0) and run on SDS-PAGE gels.

GST-mMARP1 pull-down in muscle lysate

We performed GST pull-down assays using GST-mMARP1 against mouse muscle lysate. We simultaneously exposed GST-only and GST-mMARP1 to fresh muscle lysate derived from C57BL/6J diaphragm muscles. Subsequent SDS-PAGE revealed several MARP1-binding proteins, which were submitted for identification with mass spectrometry.

Briefly, 120 µg of recombinant protein was equilibrated with 40 µl glutathione beads (Pierce, 16100) in 300 µl glutathione binding buffer (20 mM Tris HCl, 150 mM NaCl, and 10% glycerol, pH 7.5) at 4°C for 3 h. The protein-bound beads were washed with the same buffer and incubated with 5% BSA in glutathione binding buffer overnight at 4°C. The following day, mouse diaphragm lysates were prepared by lysing 30 mg of muscle tissue in 500 µl of lysis buffer containing 40 mM HEPES (pH 7.6), 120 mM NaCl, 0.5% NP-40, 10 mM NaF, 10 mM b-glycerol phosphate, 1 mM EDTA (pH 8.0), 1 mM EGTA, 2 mM sodium orthovanadate, 17 µg/ml aprotinin, 10 µg/ml leupeptin, and 1 mM PMSF, for each bait protein. Tissue was homogenized with a bullet blender x24 (Next Advance) at intensity setting 5 for four homogenization cycles (which included 2 min of blending and 2 min cooling in an ice bath), with 0.9–20.0 mm stainless steel beads (Next Advance). Cell lysates were rotated at 4°C for 20 min followed by centrifugation (13,000 *g* at 4°C for 30 min), and the clarified supernatants were used for pull-down.

The tissue supernatant was combined with the GST-mMARP1 coated glutathione beads and incubated at 4°C overnight with gentle rotation. The next day, the beads were washed five times with lysis buffer, followed by elution of the bait and binding proteins by heating at 95°C for 4 min in 15 µl SDS sample loading buffer (4% SDS, 0.0625 M Tris-HCl, 10% glycerol, 0.02% bromphenol blue, and 8 M urea). The eluate was extracted, and the beads were subjected to a second elution with fresh 15 µl SDS sample loading buffer and combined with the first elute. For one round of pull-down, we extracted the GST-MARP1 bait protein by eluting the bait and prey proteins with 8 M urea solution (50 mM Tris-HCl, 150 mM NaCl, and 8 M urea, pH 8.0) with incubation at 60°C for 10 min. GST-mMARP1 was subsequently extracted with Ni-NTA beads (Qiagen) and the flow through contained the prey proteins.

Mass spectrometry procedure was previously described (Kruse et al., 2017; Parker et al., 2019). Briefly, proteins were separated by 10% SDS-PAGE and stained with Bio-Safe Coomassie G-250 stain. One independent pull-down was used to identify three prominent prey bands and two independent pull-downs were processed to determine the MARP1 interactome. For the pull-down–based interactome experiments, each lane of the SDS-PAGE gel was cut into five slices, destained, and digested with trypsin, as previously described (Kruse et al., 2017; Parker et al., 2019). HPLC-ESI-MS/MS was performed in positive ion mode on a Thermo Scientific Orbitrap Elite Velos Pro hybrid mass spectrometer fitted with an EASY-Spray Source (Thermo Scientific). NanoLC was performed using a Thermo Scientific UltiMate 3000 RSLCnano System with an EASY Spray C18 LC column (Thermo Scientific, 50 cm × 75 µm inner diameter, packed with PepMap RSLC C18 material, 2 µm; cat. #ES803); loading phase for 15 min; mobile phase, linear gradient of 1–47% ACN in 0.1% FA in 106 min, followed by a step to 95% ACN in 0.1% FA over 5 min, held for 10 min, and then a step to 1% ACN in 0.1% FA over 1 min, and a final hold for 19 min (total run 156 min; Buffer A: 100% H_2O in 0.1% FA; Buffer B: 100% ACN in 0.1% FA; flow rate; 300 nl/min). All solvents were liquid chromatography mass spectrometry grade. Spectra were acquired using XCalibur, version 2.1.0 (Thermo Scientific). Tandem mass spectra were extracted from Xcalibur RAW files, and charge states were assigned using the ProteoWizard 2.1.x msConvert script using the default parameters. The fragment mass spectra were then

searched against the mouse SwissProt database using Mascot (Matrix Science, version 2.5.0) using the default probability cut-off score. The search variables that were used were 10 ppm mass tolerance for precursor ion masses and 0.5 D for product ion masses; digestion with trypsin; a maximum of two missed tryptic cleavages; variable modifications of oxidation of methionine and phosphorylation of serine, threonine, and tyrosine. Cross-correlation of Mascot search results with X! Tandem was accomplished with Scaffold (version Scaffold_4.4.0; Proteome Software, Portland, OR), and the Scaffold reported decoy false discovery rate. Probability assessment of peptide assignments and protein identifications were made using Scaffold. Only peptides with ≥95% probability were considered.

Actin and MARP1–N2A cosedimentation assay

We investigated MARP1 and titin N2A's ability to bind filamentous skeletal actin using a cosedimentation assay described previously (de Winter et al., 2020). Proteins were concentrated with Spin-X UF 500 5k MWCO PES concentrators (Corning), following manufacturer's instructions, to 25 µM and dialyzed into a phosphate buffer (100 mM Na_2HPO_4, 150 mM NaCl, and 10% glycerol at pH 7.5). Reagents and >99% pure rabbit skeletal actin were purchased from Cytoskeleton (Cat. #BK001 and #AKL99). Filamentous actin was prepared as described by the manufacturer. Prior to cosedimentation, the test proteins (GST-only, GST-mMARP1, SUMO-TST only, N2A [I80-81]-TST, and N2A [I80-81; Δus]-TST) were cleared from protein aggregates by centrifugation at 150,000 *g* for 1.5 h at 4°C in a Beckman TLA-120 rotor. 5 µM recombinant single or 2.5 µM combined proteins were incubated with 8 µM filamentous actin for 30 min at room temperature and cosedimented at 150,000 *g* for 1.5 h at 24°C in 2 mM $MgCl_2$, 65.3 mM NaH_2PO_4, 98 mM NaCl, 6.5% glycerol, 1,515 mM Tris HCl, pH 8.0, 60.6 µM $CaCl_2$, 16.8 mM KCl, and 1 mM ATP. Pellet and supernatant were separated and denaturized in Laemmli loading buffer (62.5 mM Tris HCl at pH6.8, 2% SDS, 10% glycerol, 5% β-mercaptoethanol, and 0.0001% Bromophenol blue). Equal amounts of both fractions were loaded onto 12% SDS-PAGE gels. Densitometric analysis was performed using ImageJ (Version 1.52a, National Institutes of Health). Western blot was performed as described below, using antibodies directed against GST and TST-tags. GST-only and SUMO-TST only were used as negative controls. The cosedimentation assay was repeated three times for each protein.

SDS gel electrophoresis and Western blotting

SDS-AGE gel electrophoresis and Western blot experiments have been previously described (Greaser and Warren, 2009; van der Pijl et al., 2018). Tissue was ground to a fine powder using Dounce homogenizers cooled in liquid nitrogen and acclimated to −20°C for 30 min before continuing. Tissue powder was resuspended in a 1:1 mixture of an 8 M urea buffer (in M; 8 urea, 2 thiourea, 0.05 Tris–HCl, 0.075 DTT, as well as 3% SDS and 0.03% Bromophenol blue, pH 6.8) and 50% glycerol containing protease inhibitors (0.04 mM E-64, 0.16 mM leupeptin, and 0.2 mM PMSF). The solutions were mixed for 4 min, followed by 10 min of incubation at 60°C. Samples were centrifuged at 12,000 rpm, and the supernatant was divided into smaller aliquots and flash frozen for storage at −80°C. SDS-AGE 1% were run on in a Hoefer SE600X vertical gel system (Hoefer Inc) was used to electrophoretically separate titin from other proteins. Gels were run at 15 mA per gel for 3 h and 15 min. For analysis of titin and MyHC levels, gels were stained using Neuhoff's Coomassie brilliant blue staining protocol. Total phosphorylation was analyzed by using Pro-Q Diamond Gel Stain and SYPRO Ruby (Thermo Fisher) for total protein. After staining, gels were scanned using a commercial scanner Gbox GBOX (Syngen). Titin migration distance and bandwidth (FWHM) were determined (see Fig. S5 for an illustration of the analysis).

Titin binding proteins MARP1–3, CAPN3, MuRF1, FHL1 and 2, or recombinant proteins and phosphorylation levels of the titin PEVK serine residues S11878 and S12022 were quantified using Western blot. For the titin binding proteins, MyHC levels were determined from Coomassie-stained initial gels to determine equalized loading for each sample and run on 2–7% acrylamide gels (van der Pijl et al., 2018). The protocol for determining phosphorylation levels of serine residues S13519 and S13663 (human, based on transcript ENSP00000467141; Ensembl TTN-214) or S12298 and S12440 (rat, based on transcript XP_017456475.1; RefSeq), better known as phospho-site S26 and S170, was previously described (Hidalgo et al., 2014). Briefly, 0.8% agarose gels were run to separate titin. Subsequently, proteins were transferred onto Immobilon-P PVDF 0.45 µm membranes (Millipore) using semi-dry transfer (Bio-Rad). Membranes were blocked with Odyssey blocking buffer (Li-Cor Biosciences) for 1 h and subsequently probed with primary antibodies at 4°C overnight. Near Infra-Red dyes were used as secondary antibodies for detection with Odyssey CLx Imaging System (Li-Cor Biosciences; for antibodies, see Table S4). Titin binding proteins were normalized against GAPDH, and phosphorylation level of S26 and S70 was normalized for total titin level by targeting the Z1Z3 domains (titin N-terminal antibody) of titin. After normalization to GAPDH, diaphragm samples of critically ill patients and of ventilated rats were compared to control samples.

Diaphragm myofiber passive force measurements

Single diaphragm muscle fibers were isolated from the biopsies, and the CSA and passive force were measured as described previously (Ottenheijm et al., 2008; Ottenheijm et al., 2012). Segments of single-diaphragm fibers of approximately 1–1.5 mm were isolated in a relaxing solution at 5°C. The diaphragm fibers were incubated for 15 min in cold (5°C) skinning solution containing relaxing solution and 1% Triton X-100 to permeabilize the plasma membrane. Subsequently, the fibers were mounted horizontally on two stainless steel hooks in a relaxing solution-filled chamber (200 µl) with a glass-coverslip bottom on the stage of an inverted microscope (Zeiss). One of the hooks was attached to a force transducer (model 403A, Aurora Scientific Inc.), which has a resonance frequency of 10 kHz, whereas the other end was attached to a servomotor (model 315C, Aurora Scientific Inc.) which has a rise time

of 250 µs. Diaphragm fiber dimensions were measured by means of a camera device coupled to the objective. Diaphragm fiber length was determined with 100× magnification; depth and width were measured with 400× magnification (an elliptical cross section of the diaphragm muscle fiber was assumed). Injury was examined microscopically; in case of damage, loss of cross striation, or other irregularities, the fibers were excluded. Diaphragm fibers were stretched to optimal length by adjusting sarcomere length to 2.5 µm using dedicated Aurora software. To ensure stable attachment of the diaphragm fiber in the clips throughout the mechanical protocol, the fiber was briefly activated prior to the experiment, and, when necessary, restretched to sarcomere length 2.5 µm. Note that this brief activation was done before the determination of diaphragm myofiber dimensions. After measuring the fiber dimensions, the stretch on the fiber was released, allowing the fiber to go back to its resting sarcomere length. After 10 min, the fiber was stretched from slack sarcomere length to a sarcomere length of 3.6 µm by a 10% length change (measured at sarcomere length 2.5 µm) per second. This accounted for an average stretch of 0.17 µm/sarcomere/s. Measurements were performed at 20°C. Data were automatically collected using a data acquisition board (sampling rate 10 kHz). Force was measured in mN or in mN/mm^2 when normalized for the cross-sectional area of the fiber for passive tension calculation. Passive tension traces were fitted with a second-order polynomial in GraphPad Prism 7. Group averages were calculated from the values obtained by the fits.

All solutions for contractile measurements had an ionic strength of 180 mM and pH 7.1. The relaxing solution had a negative logarithm of free calcium concentration of 9.0 and comprised of 5.89 mM Na_2ATP, 6.48 mM $MgCl_2$, 40.76 mM K-propionate, 100 mM BES, 6.97 mM EGTA, 14.50 mM CrP, and low concentration of freshly added protease inhibitors.

Rat mechanical ventilation

Mechanical ventilation of rats was approved by the Institutional Animal Care and Use Committee of the VU Medical Center (Amsterdam, Netherlands; protocol AVD114002016501) and the University of Arizona (Tucson, AZ; protocol 13-488). Male rats (mixed background of Sprague-Dawley/brown Norway/Fisher 344; n = 8–10) aged 5–6 mo, weighing 400–600 g were sedated and ventilated. Sedation was induced with 125 mg/kg S-ketamine (Ketanest, Pfizer) and 4 mg/kg diazepam (Centrafarm) intraperitoneally and maintained by continuous infusion of 40 mg/kg/h S-ketamine and 1 mg/kg/h diazepam intravenously. After induction, rats were endotracheally intubated with a 16-G tube, and mechanically ventilated (UMV-03, UNO) with oxygen-enriched air (40% O_2/60% N_2), 2.5 cm H_2O positive end–expiratory pressure, at ∼65 breaths/min, with a tidal volume of ∼10 ml/kg for 18 h. During this period, the respiratory rate was adjusted to maintain pH and CO_2 within physiological limits. Rats did not have visibly detectable spontaneous respiratory activity. Body temperature was maintained (36.5 ± 1.0°C) by using a warm water underbody heating pad and heating lamps. The right femoral artery was cannulated for blood sampling for blood gas analyses (ABL90, radiometer) and arterial blood pressure registration. Arterial blood pressure, electrocardiogram, and heart rate were continuously recorded using PowerLab software (Chart 8.0; ADInstruments). After 18 h of ventilation, the rats were sacrificed by exsanguination and the whole diaphragm was snap frozen in liquid nitrogen and stored at −80°C until used for protein analysis. As a control group, eight rats were briefly ventilated (≤15 min) before the diaphragm was excised.

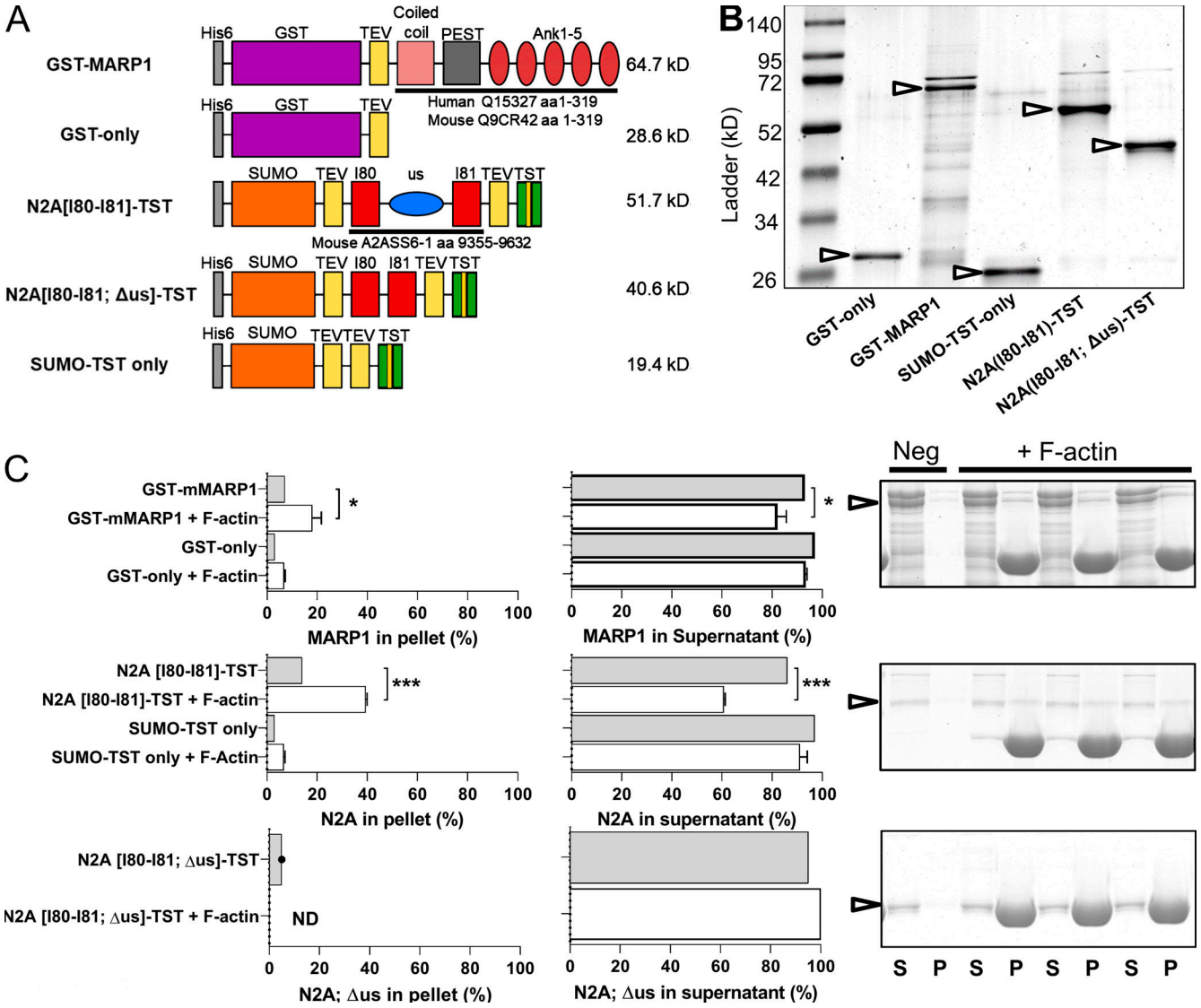

Figure S1. **Recombinant constructs and results of F-actin cosedimentation assays with GST-mMARP1 and N2A[I80-I81]-TST. (A)** Graphic representations of the recombinant protein constructs. **(B)** Representative gel of the recombinant proteins (arrows). **(C)** Quantification and representative gel images of cosedimentation with F-actin. Top: GST-mMARP1 sediments with F-actin in the pellet (P) fraction with a concomitant decrease in the supernatant (S) fraction. Similar results were found for N2A[I80-I81]-TST (middle), while N2A[I80-I81; Δus]-TST (bottom) did not interact with F-actin, suggesting that the unique sequence of N2A between I80-I81 is required for binding to the actin thin filament. Cosedimentation of the tag-only proteins did not show interaction with F-actin. Bars denote mean ± SD; three replicates for each cosedimentation assay. *T* test relative to no F-actin; *, $P < 0.05$; ***, $P < 0.001$.

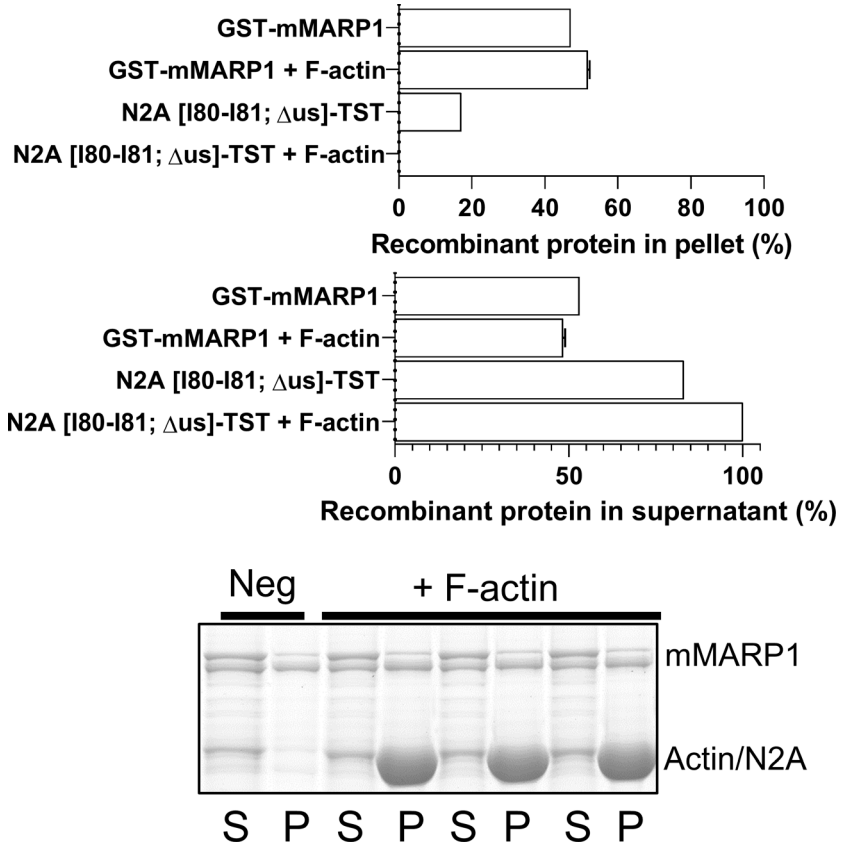

Figure S2. **F-actin cosedimentation of the GST-mMARP1 and N2A[I80-I81; Δus]-TST complex.** Cosedimentation of GST-mMARP1 and N2A[I80-I81; Δus]-TST with F-actin, showed similar levels of MARP1 in the pellet (P) and supernatant (S) fraction compared with GST-mMARP1 alone (Fig. S1 D), suggesting that the unique sequence of N2A is required to enhance the binding affinity of GST-mMARP1 in complex with N2A to F-actin (see Fig. 3 D). Bars denote mean ± SD; three replicates for each cosedimentation assay.

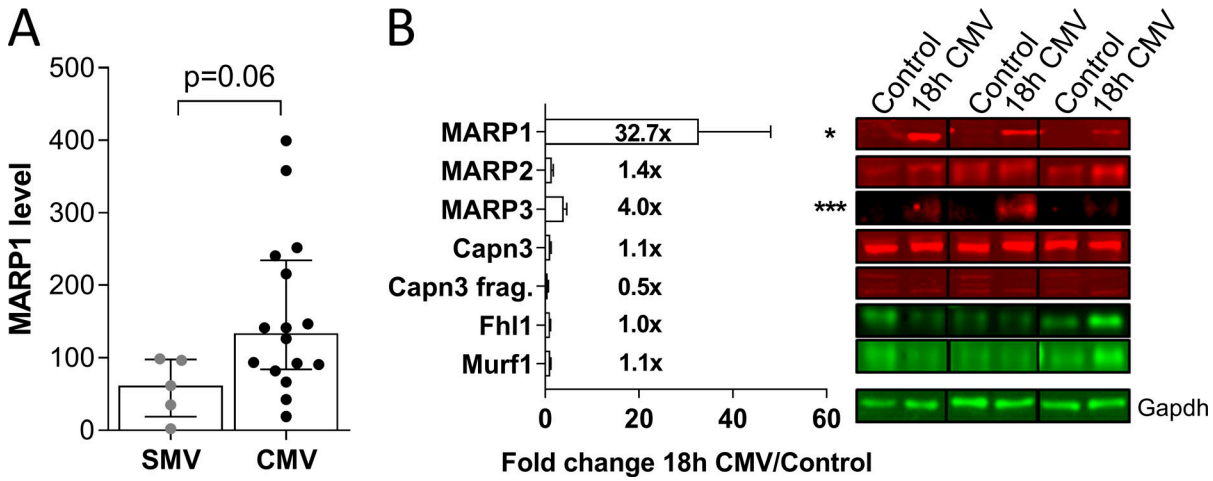

Figure S3. **MARP1 levels in supported and controlled mechanically ventilated critically ill patients, and expression of titin-binding proteins in 18 h CMV rats. (A)** Critically ill patients on CMV tended to have higher MARP1 levels than patients ventilated with a supportive mode (SMV; (*t* test; P = 0.06). **(B)** Representative examples of Western blots stained with antibodies against MARP1-3, FHL1, CAPN3, MuRF1, and GAPDH. MARP1 was markedly up-regulated in diaphragm myofibers of rats who were mechanically ventilated (CMV) for 18 h (*n* = 8; controls *n* = 10). Data are presented as mean ± SEM. FHL, four-and-a-half LIM domains protein 1; MuRF1, muscle ring finger protein 1; CAPN3, calpain 3; Frag, fragment. *T* test relative to controls; *, P < 0.05; ***, P < 0.001.

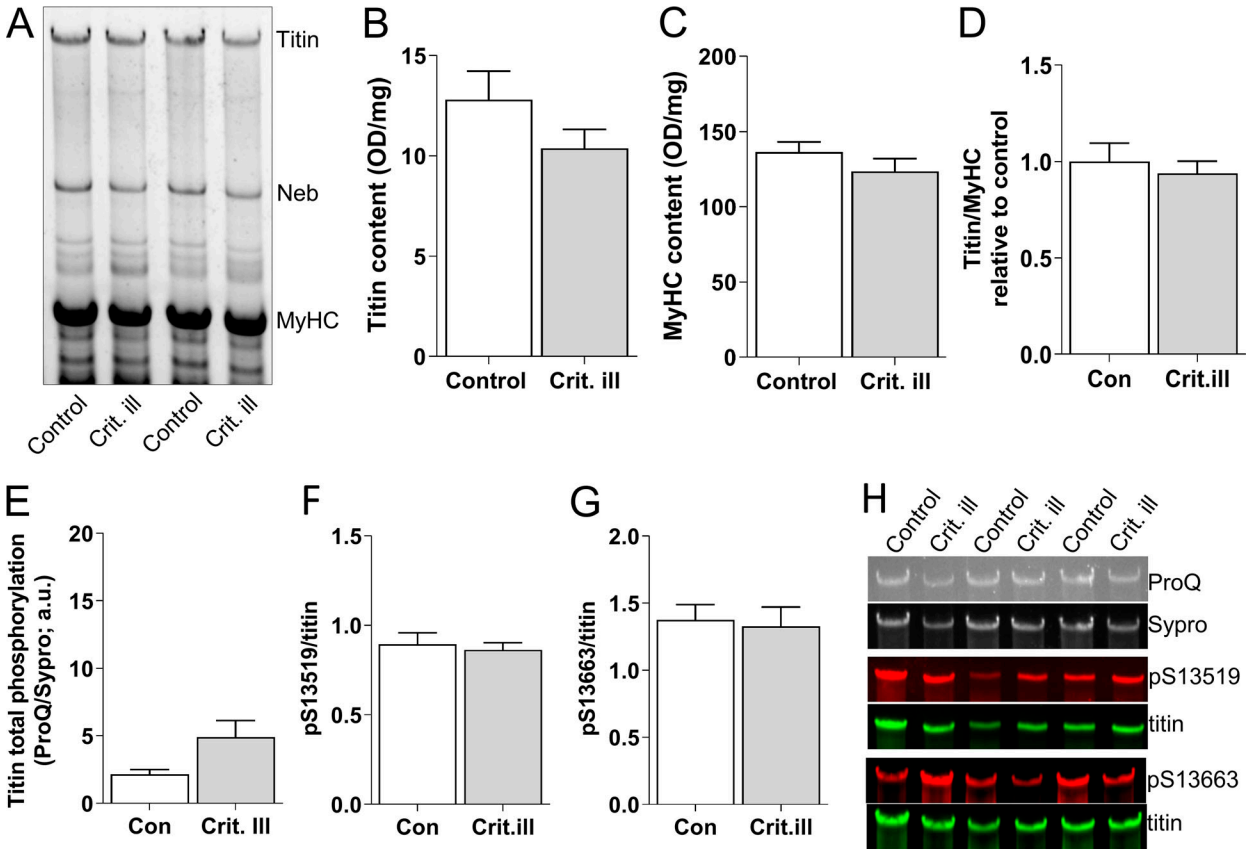

Figure S4. **Relative titin protein and phosphorylation levels in critically ill patients compared to controls. (A)** Representative example of an SDS-AGE gel with critically ill (n = 21) and control (n = 18) diaphragm samples. **(B)** Titin content is comparable between critically ill and control patients. **(C)** Myosin heavy chain (MyHC) content, normalized to diaphragm tissue wet weight, is comparable between critically ill and control patients. **(D)** Ratio of titin/MyHC was comparable between control and critically ill patients. **(E)** Total phosphorylation levels, as assessed by ProQ Diamond staining normalized to Sypro Ruby staining, was comparable between control and critically ill patients. **(F and G)** Phosphorylation of S13519 (S26) and S13663 (S170) in the PEVK region of titin (phosphorylation of these sites is known to increase titin stiffness) was comparable between critically ill and control patients. **(H)** Examples of stainings with ProQ Diamond, Sypro Ruby, and antibodies against phosphorylated S13519 (S26) and S13663 (S170) in the PEVK region of titin. Bars denote mean ± SEM.

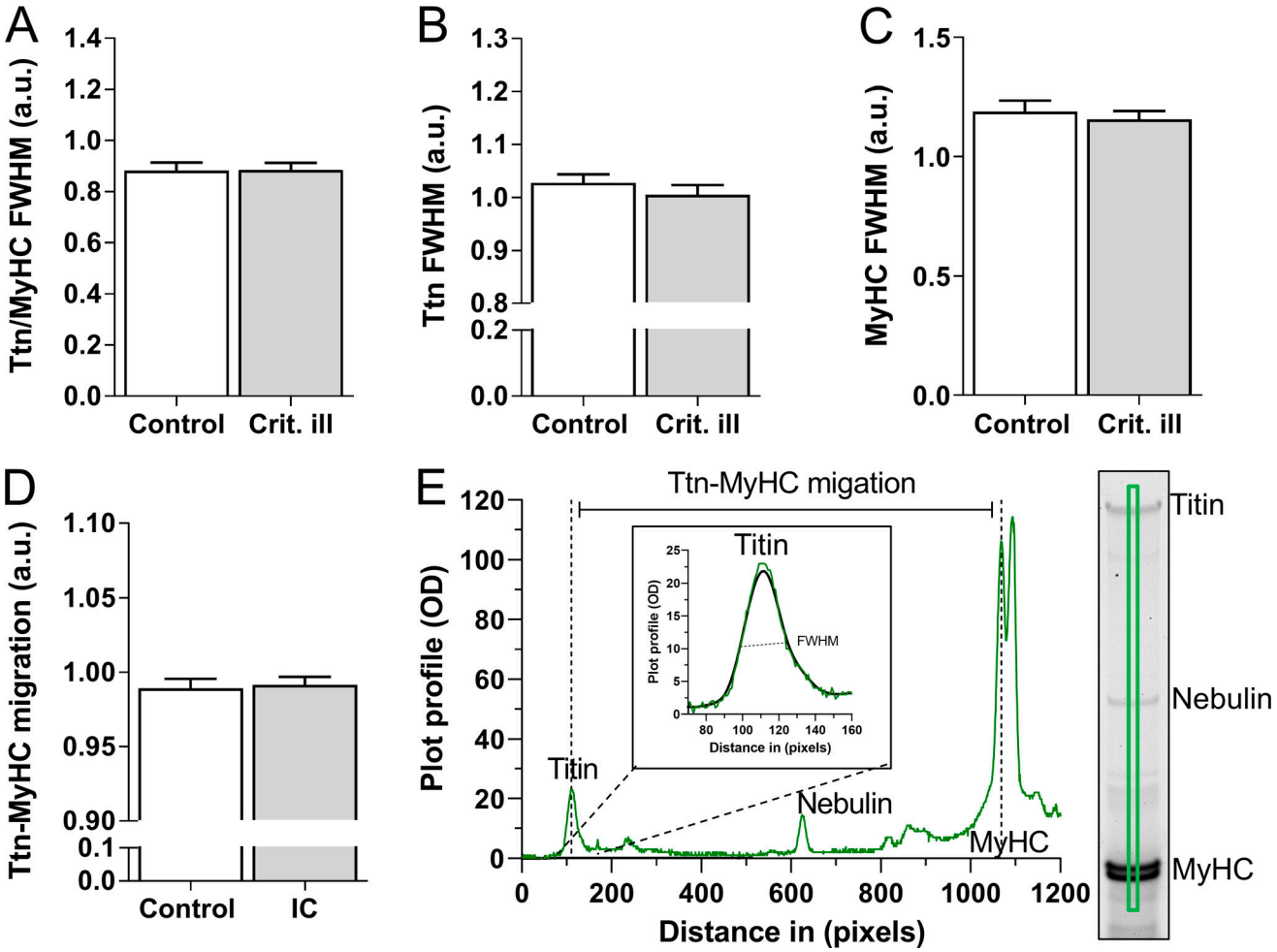

Figure S5. **Titin isoform size and splice variation in human diaphragm biopsies.** Control (n = 16) and critically ill (n = 21) patient samples were migrated on SDS-AGE gels; bandwidth was determined by generating plot-profiles fitted with Gaussian fits to generate FWHM for titin and myosin heavy chain (MyHC) bands. **(A–C)** FWHM of titin/MyHC (A), raw titin (B), and MyHC (C) values, showing no difference in bandwidth, suggesting similar levels of titin isoforms present in both control and critically ill patients. **(D)** Migration distance of titin to MyHCII, suggesting little or no difference in titin splicing. **(E)** Example plot profile, explaining the FWHM and migration measurements. Graph A–D represented as mean ± SD. A reference sample was run on each gel and used to normalize for variations in bandwidth and migration between gels. Bars denote mean ± SEM.

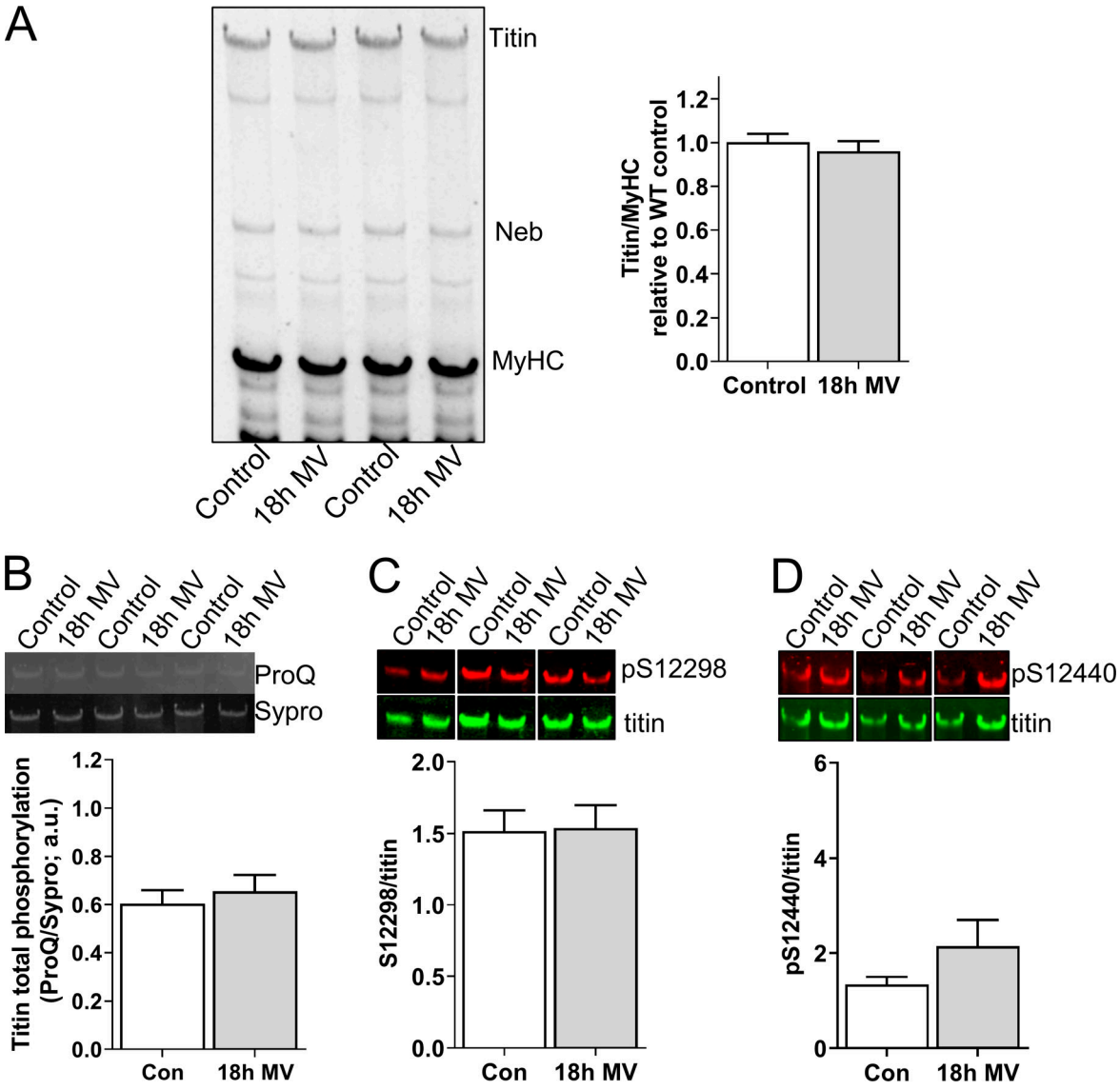

Figure S6. **Relative titin protein and phosphorylation levels in 18 h ventilated and control rats. (A)** Left: Representative example of a SDS-AGE gel with diaphragm samples of control (n = 10) and mechanically ventilated (MV, 18 h; n = 8) rats. Right: Ratio of titin/MyHC was comparable between control and ventilated rats. **(B)** Total phosphorylation levels, as assessed by ProQ Diamond staining normalized to Sypro Ruby staining, was comparable between control and ventilated rats. **(C and D)** Phosphorylation of S13519 (S26) and S13663 (S170) in the PEVK region of titin (phosphorylation of these sites is known to increase titin stiffness) was comparable between control and ventilated rats. Bars denote mean ± SEM.

Four tables are provided online. Table S1 contains summarized patient information pertaining to medical history and mechanical ventilation settings. Table S2 contains mass spectrometry data of identified proteins from pull-down assays. Table S3 shows primer data used in this paper. Table S4 displays antibodies used in this paper.